nature medicine

MicroRNA-148a regulates LDL receptor and ABCA1 expression to control circulating lipoprotein levels

Leigh Goedeke[1–4], Noemi Rotllan[1,2,12], Alberto Canfrán-Duque[1,2,12], Juan F Aranda[1–3], Cristina M Ramírez[1,2], Elisa Araldi[1–4], Chin-Sheng Lin[3,4], Norma N Anderson[5,6], Alexandre Wagschal[7,8], Rafael de Cabo[9], Jay D Horton[5,6], Miguel A Lasunción[10,11], Anders M Näär[7,8], Yajaira Suárez[1–4] & Carlos Fernández-Hernando[1–4]

The hepatic low-density lipoprotein receptor (LDLR) pathway is essential for clearing circulating LDL cholesterol (LDL-C). Whereas the transcriptional regulation of LDLR is well characterized, the post-transcriptional mechanisms that govern LDLR expression are just beginning to emerge. Here we develop a high-throughput genome-wide screening assay to systematically identify microRNAs (miRNAs) that regulate LDLR activity in human hepatic cells. From this screen we identified and characterized miR-148a as a negative regulator of LDLR expression and activity and defined a sterol regulatory element–binding protein 1 (SREBP1)-mediated pathway through which miR-148a regulates LDL-C uptake. In mice, inhibition of miR-148a increased hepatic LDLR expression and decreased plasma LDL-C. Moreover, we found that miR-148a regulates hepatic expression of ATP-binding cassette, subfamily A, member 1 (ABCA1) and circulating high-density lipoprotein cholesterol (HDL-C) levels *in vivo*. These studies uncover a role for miR-148a as a key regulator of hepatic LDL-C clearance through direct modulation of LDLR expression and demonstrate the therapeutic potential of inhibiting miR-148a to ameliorate an elevated LDL-C/HDL-C ratio, a prominent risk factor for cardiovascular disease.

The hepatic LDLR is crucial for maintaining cholesterol homeostasis. Reduced LDLR expression leads to decreased LDL catabolism and elevated levels of plasma LDL-C, a strong risk factor for cardiovascular disease in humans[1,2]. LDLR expression is tightly and coordinately regulated. The transcription of LDLR is coupled to intracellular levels of cholesterol by two major regulatory pathways, the SREBPs and the liver X receptors (LXRs)[3,4]. SREBPs bind to sterol regulatory elements (SREs) and promote target gene expression[3]. In mammals there are three SREBP isoforms: SREBP1a and SREBP1c, which are encoded by the *SREBF1* gene, and SREBP2, which is encoded by the *SREBF2* gene[5–7]. SREBP1c is regulated by insulin, oxysterols and phosphatidylcholine and preferentially enhances the transcription of genes involved in fatty acid, phospholipid and triacylglycerol synthesis; in contrast, SREBP2 and SREBP1a are regulated by intracellular cholesterol[3,8,9]. SREBP2 is the main regulator of *de novo* cholesterol biosynthesis and uptake. When intracellular cholesterol levels are low, the SREBP2 precursor traffics from the endoplasmic reticulum (ER) to the Golgi where it is processed to its mature, nuclear form that switches on the transcription of genes involved in cholesterol biosynthesis (such as 3-hydroxy-3-methylglutaryl-CoA reductase (*HMGCR*), which encodes the rate-limiting enzyme of cholesterol biosynthesis) and genes involved in cholesterol uptake (such as *LDLR*)[3,8]. SREBPs also control the expression of proprotein convertase subtilisin/kexin type 9 (PCSK9), a protein involved in the post-transcriptional degradation of LDLR[10,11]. Conversely, during sterol-replete conditions, the SREBP2 precursor is retained in the ER and can no longer be processed. Under these conditions the nuclear receptor superfamily member, LXR, is activated by oxysterols and induces the expression of genes involved in cholesterol efflux, such as the ATP-binding cassette (ABC) transporters *ABCA1* and *ABCG1* (ref. 12). Additionally, LXR controls cholesterol homeostasis through upregulation of the E3 ubiquitin ligase inducible degrader of LDLR (IDOL), which triggers the ubiquitination and degradation of LDLR, thereby preventing reuptake of cholesterol and completing the feedback loop[4].

miRNAs are short (~22 nt), evolutionarily conserved, single-stranded RNAs that control the expression of mRNAs with complementary target sequences, leading to their transcript destabilization, translational inhibition or both[13–15]. Recently several laboratories, including ours, have demonstrated that miRNAs are a

[1]Vascular Biology and Therapeutics Program, Yale University School of Medicine, New Haven, Connecticut, USA. [2]Integrative Cell Signaling and Neurobiology of Metabolism Program, Section of Comparative Medicine, Yale University School of Medicine, New Haven, Connecticut, USA. [3]Department of Medicine, Leon H. Charney Division of Cardiology, New York University School of Medicine, New York, New York, USA. [4]Department of Cell Biology, New York University School of Medicine, New York, New York, USA. [5]Department of Molecular Genetics, University of Texas Southwestern Medical Center, Dallas, Texas, USA. [6]Department of Internal Medicine, University of Texas Southwestern Medical Center, Dallas, Texas, USA. [7]Massachusetts General Hospital Cancer Center, Charlestown, Massachusetts, USA. [8]Department of Cell Biology, Harvard Medical School, Boston, Massachusetts, USA. [9]Translational Gerontology Branch, National Institute on Aging, National Institutes of Health, Baltimore, Maryland, USA. [10]Servicio de Bioquímica-Investigación, Hospital Universitario Ramón y Cajal, Instituto Ramón y Cajal de Investigación Sanitaria, Madrid, Spain. [11]Centro de Investigación Biomédica en Red Fisiopatología de la Obesidad y Nutrición, Madrid, Spain. [12]These authors contributed equally to this work. Correspondence should be addressed to C.F.-H. (carlos.fernandez@yale.edu).

Received 7 May; accepted 20 August; published online 5 October 2015; doi:10.1038/nm.3949

critical component of the cholesterol regulatory circuitry, e.g., miR-33 cooperates with its host *SREBF* genes in a negative feedback loop to regulate intracellular lipid levels, whereas the SREBP2-induced cluster of miR-96, miR-182 and miR-183 controls cholesterol homeostasis by affecting nuclear SREBP accumulation[16–18]. A number of miRNAs that control lipid metabolism *in vivo* have also been identified (such as miR-122, miR-30c, miR-33a, miR-33b, miR-144 and miR-223). In particular, studies of miR-33, miR-144 and miR-223 demonstrate the crucial role of miRNAs in regulating cellular cholesterol efflux and HDL biogenesis[19–24]. miR-122, whose expression is highly restricted to the liver, has been linked to the regulation of cholesterol and fatty acid synthesis through loss-of-function experiments in both mice and nonhuman primates[25–27], and miR-30c regulates lipoprotein assembly by targeting the microsomal triglyceride transfer protein (MTP), a protein that is crucial for the assembly of apolipoprotein B (APOB)-containing lipoproteins[28]. Although these studies highlight the therapeutic potential of manipulating miRNAs to control HDL-C levels, cholesterol biosynthesis and very-low-density lipoprotein (VLDL) secretion, the effects of miRNAs on LDLR activity, and thus on LDL-C, remain poorly understood.

RESULTS

Primary miRNA screen design and optimization

To systematically identify miRNAs that regulate LDLR activity, we developed a high-throughput microscope-based screening assay to monitor the effect of miRNA overexpression on 3,3′-dioctadecylindocarbocyanine-LDL (DiI-LDL) uptake in human hepatic (Huh7) cells (**Fig. 1a**). To avoid the confounding effects of the lipoproteins in the media, we initially characterized the specific uptake of DiI-LDL in Huh7 cells incubated in 10% lipoprotein-deficient serum (LPDS). After treatment of the cells with increasing concentrations of DiI-LDL for 8 h, we measured cell-associated DiI fluorescence by flow cytometry. DiI-LDL uptake kinetics were saturable and showed complete saturation at approximately 20–40 μg/ml DiI–LDL-C (**Supplementary Fig. 1a**,**b**), in accordance with the well-known kinetic properties of the LDLR[29,30]. Similar results were observed when we cultured cells in 384-well plates and measured fluorescence intensity using automated fluorescence microscopy (**Supplementary Fig. 1c**). As expected, LDL uptake was specific, as DiI-LDL accumulation was reduced when cells were incubated in the presence of a 30-fold excess of unlabeled LDL (**Supplementary Fig. 1d**). We further analyzed whether our system was suitable for functional genomic studies by assessing *LDLR* gene inactivation by RNA interference (RNAi). Notably, treatment of Huh7 cells with an siRNA directed against *LDLR* (siLDLR) substantially reduced LDLR expression at the protein level (**Supplementary Fig. 1e**) and diminished DiI-LDL uptake (**Supplementary Fig. 1f**,**g**). The *Z′*-factor (which is a measure of statistical effect size in high-throughput screenings) was > 0.5 (**Supplementary Fig. 1f**), indicative of a robust screen[31].

Identification of miRNAs that regulate LDLR activity

For the genome-wide miRNA screen, Huh7 cells were transfected in triplicate with a library of 1,719 distinct miRNA mimics and incubated with 30 μg/ml DiI–LDL-C. After 8 h of incubation, the cells were washed, fixed and stained with Hoechst dye (**Fig. 1a**). In addition to the internal controls that were included with each screening replicate (see Online Methods), previously validated siRNAs against *LDLR* and a nonsilencing control siRNA were used as positive and negative controls, respectively (**Supplementary Fig. 1f**,**g**). The mean average intensity of DiI-LDL uptake was determined on an individual-cell basis using automated high-content image analysis software. To standardize measurements from different plates, the phenotypic effects of each miRNA that increased or decreased average DiI intensity were converted to robust *z*-scores on the basis of the median average intensity of each array plate[32]. Notably, comparisons of plate replicates and internal plate controls indicated high reproducibility of the screen (**Fig. 1b**,**c**). Upon normalization, robust *z*-scores for each individual miRNA were ranked and compared to their respective plate replicates (**Supplementary Table 1**). Whereas the screen identified miRNAs that increased or decreased LDL uptake, we chose to focus on miRNAs whose overexpression decreased receptor activity, as pharmacological inhibitors of this miRNA subset represent potential therapeutic agents to lower LDL-C levels.

To narrow down candidates, we designed a multistep system in which miRNAs were subjected to four screening passes before being chosen for further validation (**Fig. 1a**). In the first pass, a miRNA was

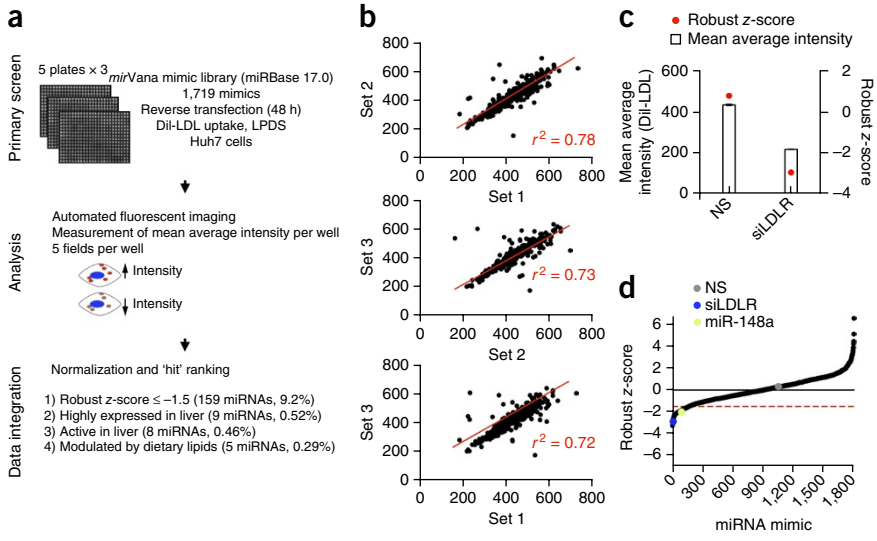

Figure 1 Genome-wide miRNA screen identifies novel regulators of LDLR activity. (**a**) Schematic workflow of the primary screen and the bioinformatic analysis. 1,719 miRNA mimics arrayed in five plates were screened in triplicate (5 plates × 3). (**b**) Linear regression analysis of DiI-LDL mean average intensity (MAI) for plate sets 1 and 2 (top), plate sets 2 and 3 (middle) and plate sets 1 and 3 (bottom). The goodness-of-fit (r^2) and regression line (indicative of overall reproducibility of the screen) are indicated in red on each graph. (**c**) Comparison of DiI-LDL MAI (open bars) and robust *z*-score (red dots) for cells transfected with a negative-control siRNA (nonsilencing, NS) or positive-control siRNA (siRNA to *LDLR*, siLDLR). (**d**) Distribution of average robust *z*-scores for individual miRNAs in the primary screen. Controls are NS siRNA (gray dot) and siLDLR (blue dot). miR-148a (yellow dot) was chosen for further validation on the basis of predefined criteria (outlined in **a**). All other miRNAs are shown as black dots. Dashed red line, robust *z*-score = –1.5.

considered to be a putative regulator of LDLR activity if it reduced DiI-LDL fluorescence (robust z-score ≤ −1.5) in at least two of the replicate screening plates (**Fig. 1d**). Although this criterion is less stringent than most cut-offs for high-throughput screenings[32], this pass was designed to yield a substantially higher hit rate (159 miRNAs, ~9.2% of miRNAs screened) to allow for subsequent screening passes (**Supplementary Table 1**).

To minimize the risk of identifying false positives, the ensuing screening passes required the candidate miRNAs to be highly expressed in human and/or mouse liver, to be active in the liver (i.e., increased miRNA expression is associated with reduced target gene expression) and to be modulated by dietary lipids (**Fig. 1a**). Of the 159 miRNAs identified from the initial pass, five miRNAs (miR-140, miR-128, miR-148a, miR-148b and miR-193b; ~0.29% of miRNAs screened) met these cut-offs, with miR-148a emerging as a strong positive hit—showing medium-to-high expression in human and mouse hepatic tissues[33–35], high liver activity[36] and differential expression in the livers of mice fed a high-fat diet (HFD)[35] (**Supplementary Table 2**). Of note, it has recently been shown that single-nucleotide polymorphisms (SNPs) in the promoter region of *MIR148A* are associated with altered LDL-C and triglyceride levels in humans[37–39], suggesting a possible physiological role for this miRNA in regulating lipid metabolism and highlighting this miRNA for further study.

miR-148a expression is regulated by hepatic lipid content

MIR148A is encoded within an intergenic region of human chromosome 7 and is highly conserved among vertebrate species (**Supplementary Fig. 2a**). In agreement with previous reports[35], *Mir148a* was highly expressed in mouse liver (**Supplementary Fig. 2b**) and was upregulated in the livers of HFD-fed mice (**Supplementary Fig. 2c**). Additionally, we found that the expression of *Mir148a* was substantially increased in the livers of HFD-fed rhesus monkeys (**Supplementary Fig. 2d**). In accordance with this result, and consistent with previous observations[40], the mature form of *Mir148a* was also markedly upregulated in the livers of leptin-deficient genetically obese (*ob*/*ob*) mice (**Supplementary Fig. 2e**).

To gain insight into the functional role of miR-148a in cholesterol homeostasis, we analyzed its potential targets using a rigorous bioinformatic algorithm[41]. Predicted targets identified by three target-prediction websites (TargetScan, miRWalk and miRanda)[42–44] were assigned to functional annotation clusters using the public gene ontology database DAVID[45]. As shown in **Supplementary Table 3**, miR-148a target genes were enriched ($E \geq 1.0$) within 78 clusters and several annotation networks. This functional cluster analysis was combined with data on known and predicted associations between individual miR-148a target genes that are enriched in lipid metabolism using the STRING v9 (ref. 46) and PANTHER databases[47]. From this bioinformatic analysis (**Supplementary Fig. 3a**), miR-148a

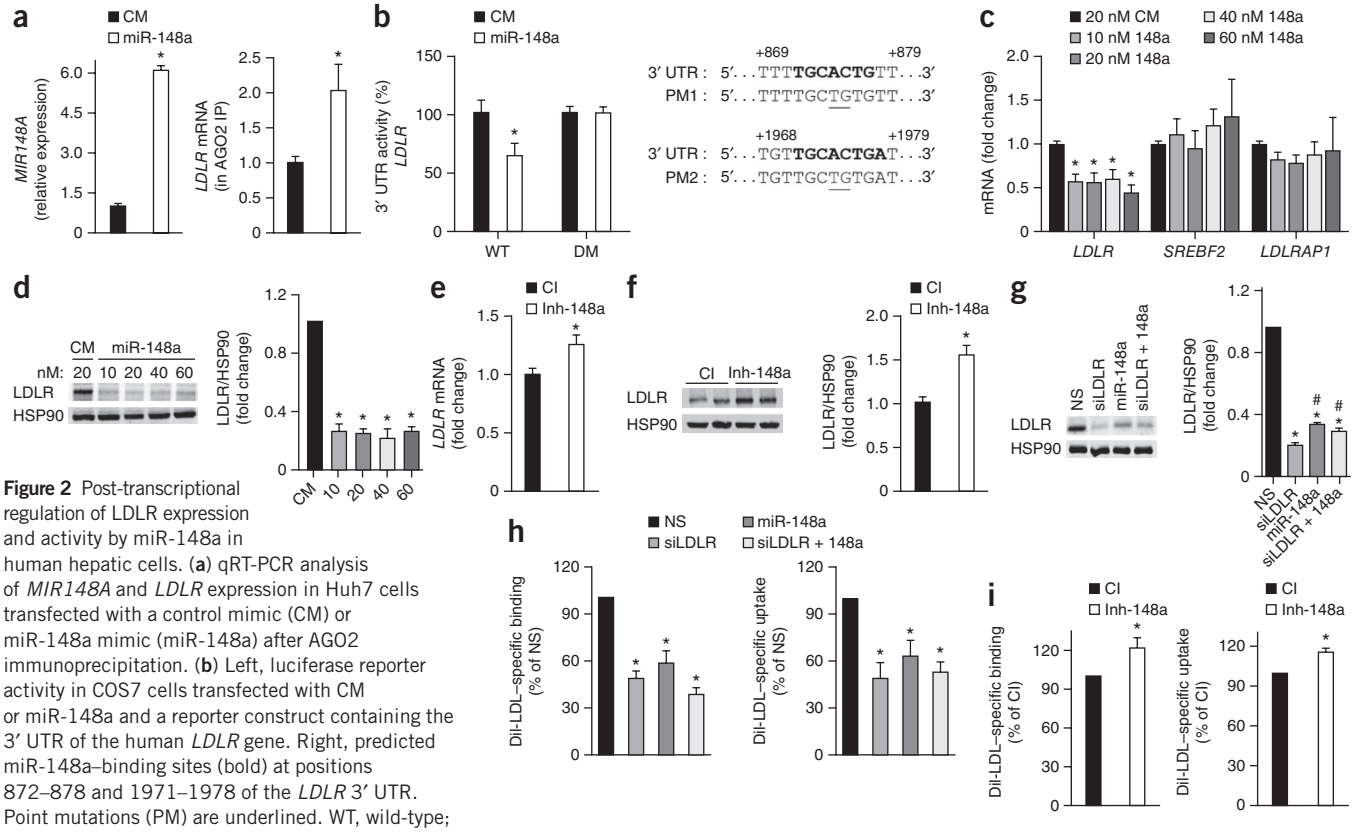

Figure 2 Post-transcriptional regulation of LDLR expression and activity by miR-148a in human hepatic cells. (**a**) qRT-PCR analysis of *MIR148A* and *LDLR* expression in Huh7 cells transfected with a control mimic (CM) or miR-148a mimic (miR-148a) after AGO2 immunoprecipitation. (**b**) Left, luciferase reporter activity in COS7 cells transfected with CM or miR-148a and a reporter construct containing the 3′ UTR of the human *LDLR* gene. Right, predicted miR-148a–binding sites (bold) at positions 872–878 and 1971–1978 of the *LDLR* 3′ UTR. Point mutations (PM) are underlined. WT, wild-type; DM, double mutant. (**c**,**d**) qRT-PCR for *LDLR*, *SREBF2* and *LDLRAP1* (**c**) and representative western blot analysis of LDLR (**d**) in Huh7 cells transfected with CM or the indicated concentrations of miR-148a (148a). Heat shock protein 90 (HSP90) was used as a loading control. (**e**,**f**) qRT-PCR (**e**) and representative western blot analysis (**f**) of LDLR in Huh7 cells transfected with a control inhibitor (CI) or an inhibitor of miR-148a (Inh-148a). HSP90 was used as a loading control. (**g**,**h**) Representative western blot (**g**) and flow cytometry analysis of DiI-LDL binding and uptake (**h**) in Huh7 cells transfected with nonsilencing (NS) siRNA, miR-148a mimic, siRNA against *LDLR* (siLDLR) or both miR-148 mimic and siLDLR. $^{*}P \leq 0.05$ compared to NS-transfected cells by one-way analysis of variance (ANOVA). $^{\#}P \leq 0.05$ compared to siLDLR-transfected cells by one-way ANOVA with Bonferroni correction for multiple comparisons. (**i**) Flow cytometry analysis of DiI-LDL binding and uptake in Huh7 cells transfected with CI or Inh-148a. In **a**,**c**–**i**, data are the mean ± s.e.m. of ≥3 experiments in duplicate. In **b** data are the mean ± s.e.m. of ≥3 experiments in triplicate. $^{*}P \leq 0.05$ compared to CM- or CI-transfected cells by unpaired t-test (**a**–**f**,**i**).

potentially controls a vast network of lipid metabolism regulators, including the LDLR.

miR-148a inhibits LDLR expression and regulates LDLR activity

We identified two predicted binding sites for miR-148a in the 3′ untranslated region (UTR) of *LDLR*, one of which is conserved in mammals (**Supplementary Fig. 3b**). To assess the effect of miR-148a on *LDLR* expression, we first performed ribonucleoprotein immunoprecipitation (RNP-IP) using an antibody specific to argonaute-2 (AGO2), a component of the RNA-induced silencing complex (RISC) that mediates miRNA-directed gene silencing. Overexpression of miR-148a significantly enriched the association of *LDLR* mRNA with the AGO2-containing complex (**Fig. 2a**), suggesting that LDLR expression is directly regulated by miR-148a. Additionally, overexpression of miR-148a markedly reduced *LDLR* 3′ UTR activity as compared to that in control-transfected cells (**Fig. 2b**). Notably, combined mutation of the two miR-148a target sites relieved miR-148a–mediated repression of *LDLR* 3′ UTR activity (**Fig. 2b**). We then determined the effect of miR-148a on LDLR mRNA and protein expression. Transfection of Huh7 cells with miR-148a, but not with a control mimic (CM), significantly decreased LDLR mRNA and protein levels (**Fig. 2c**,**d**), and the effects of miR-148a were seen at concentrations as low as 10 nM (**Fig. 2c**,**d**). A miR-148a mimic that is mutated in the seed sequence (CM*) was used as a negative control (**Supplementary Fig. 4a**). The inhibition of *LDLR* expression by miR-148a was highly specific because the expression of other cholesterol-related genes, such as *SREBF2* and LDLR adapter protein 1 (*LDLRAP1*), was not influenced by miR-148a overexpression (**Fig. 2c**). Notably, inhibition of endogenous miR-148a in Huh7 cells significantly increased the expression of LDLR as compared to that in cells transfected with a control inhibitor (CI) (**Fig. 2e**,**f**). We observed similar results in another human hepatic cell line, HepG2, as well as in mouse hepatic (Hepa) cells (**Supplementary Fig. 4b–e**). Finally, we found that miR-148a overexpression did not cause a further decrease in LDLR levels in Huh7 cells transfected with siLDLR (**Fig. 2g**).

Defective hepatic LDLR activity results in elevated levels of LDL-C in the blood and is associated with an increased risk of coronary artery disease[1,2]. To assess the role of miR-148a in regulating LDL-C uptake in human and mouse hepatic cells, we overexpressed or inhibited miR-148a and assessed DiI-LDL binding and uptake by flow cytometry. Transfection of Huh7, HepG2 and Hepa cells with miR-148a attenuated DiI-LDL–specific binding (**Fig. 2h** and **Supplementary Fig. 4f**) and uptake (**Fig. 2h** and **Supplementary Fig. 4g**), whereas transfection with an miR-148a antagonist (Inh-148a) increased DiI-LDL–specific binding and uptake (**Fig. 2i** and **Supplementary Fig. 4h**,**i**). These effects appear to be mediated by the direct targeting of LDLR expression by miR-148a, because *LDLR* silencing abrogated the effect of miR-148a overexpression on DiI-LDL binding and uptake (**Fig. 2h**). Additionally, when we analyzed internalization of an antibody specific to LDLR and DiI-LDL uptake by immunofluorescence, we observed reduced LDLR internalization and a concomitant decrease in DiI-LDL uptake in Huh7 cells overexpressing miR-148a as compared to cells transfected with a negative control mimic (**Fig. 3a**,**b**). Consistent with these results, transfection of Huh7 cells with miR-148a significantly reduced the intracellular cholesterol concentration after incubation with unlabeled native LDL (nLDL) as compared to that in CM-treated cells (**Fig. 3c**). Notably, the intracellular cholesterol concentration was increased in Huh7 cells overexpressing an inhibitor of miR-148a (**Fig. 3d**), confirming the endogenous role of miR-148a in modulating cholesterol uptake.

We next determined whether the effect of miR-148a in regulating LDL binding and uptake could be rescued by overexpressing an LDLR-GFP cDNA construct lacking the 3′ UTR, which is thereby resistant to the inhibitory action of miR-148a. The significant reduction in DiI-LDL binding and uptake induced by miR-148 in Huh7 cells, as analyzed by immunofluorescence, was abrogated in cells that expressed the LDLR-GFP construct (**Fig. 3e**,**f**). In these experiments, transfection of the LDLR-GFP construct led to massively increased DiI-LDL binding and uptake. However, these results, together with

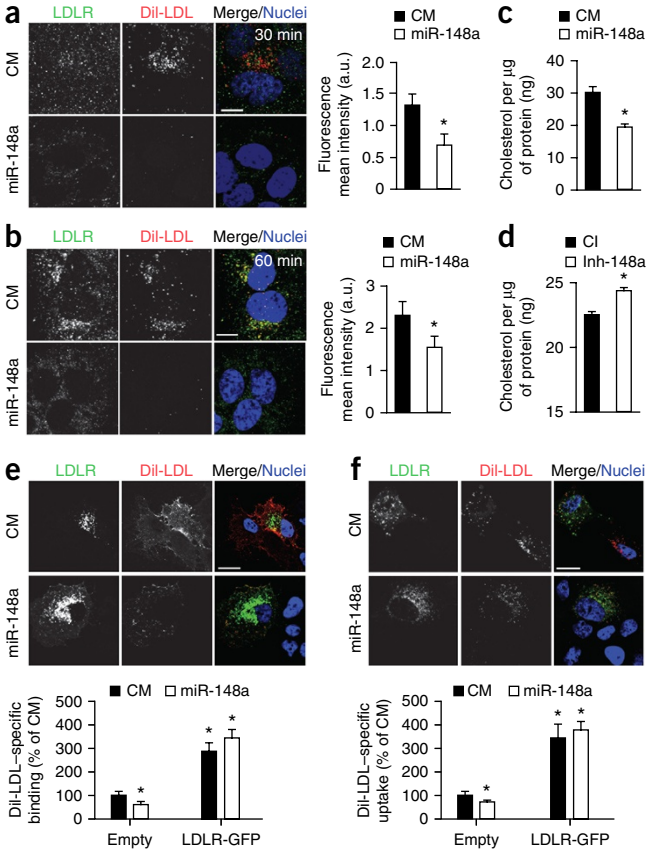

Figure 3 LDLR-GFP overexpression rescues LDLR activity in miR-148a–transfected cells. (**a**,**b**) LDLR antibody internalization in Huh7 cells transfected with a control mimic (CM) or miR-148a mimic (miR-148a) and incubated with anti-LDLR and 30 µg/ml of DiI-LDL for 40 min at 4 °C. After internalization at 37 °C for 30 min (**a**) or 60 min (**b**) at 37 °C, cells were washed, fixed and stained. Red, DiI-LDL; green, LDLR; blue, nuclei stained with TO-PRO-3 iodide (TOPRO). Scale bars, 5 µm. Quantification of DiI-LDL mean intensity is shown on the right. (**c**,**d**) Intracellular cholesterol content in Huh7 cells transfected with CM or miR-148a (**c**) or control inhibitor (CI) or miR-148a inhibitor (Inh-148a) (**d**) and incubated with 30 µg/ml native LDL (nLDL) for 2 h. (**e**,**f**) DiI-LDL binding (**e**) and uptake (**f**) in Huh7 cells co-transfected with LDLR-GFP or control vector (empty) and CM or miR-148a. Red, DiI-LDL; green, LDLR; blue, TOPRO. Scale bars, 10 µm. Quantification by flow cytometry is shown below the micrographs. $^*P \leq 0.05$ by comparison with data from cells transfected with CM by one-way ANOVA with Bonferroni correction for multiple comparisons. In **a**,**b**,**e**,**f**, images are representative of ≥3 experiments that gave similar results. In **c**–**f**, data are the mean ± s.e.m. and representative of ≥3 experiments in duplicate. $^*P \leq 0.05$ compared to CM- or CI-transfected cells by unpaired *t*-test (**a**–**d**). a.u., arbitrary units.

our previous observation that miR-148a overexpression does not influence DiI-LDL uptake in cells transfected with siLDLR (**Fig. 2h**), suggest that miR-148a regulates DiI-LDL binding and uptake by direct downregulation of LDLR expression. Alternatively, miR-148a could be acting upstream or downstream of LDLR. Taken together, these results demonstrate that manipulation of cellular levels of miR-148a alters LDLR activity.

Transcriptional regulation of miR-148a by SREBP1c

Given that miR-148a levels are regulated by dietary lipids[35], we next sought to determine how this miRNA is transcriptionally regulated. Previous computational methods have identified several transcriptional start sites (TSSs) located ~1.1 to ~1.6 kb upstream of the *MIR148A* sequence[48,49]. Notably, these TSSs correlate with epigenetic signatures and adjacent active promoter and enhancer regions that are involved in the regulation of *MIR148A* expression[50,51] (**Supplementary Fig. 5a**). Intriguingly, using chromatin immunoprecipitation combined with massively parallel sequencing (ChIP-seq), an SREBP1-binding site as well as binding sites for generic transcription factors involved in SREBP1 activation (Sp1 and Nfy) were previously identified in the adjacent active promoter region of miR-148a (ref. 52). Additionally, we identified several other conserved SREBP1-binding sites (E-box elements, 5′-CANNTG-3′) using target-prediction algorithms (**Supplementary Fig. 5b**). As it has been reported that SREBP1c is increased in the livers of *ob*/*ob* mice and under HFD-fed conditions[53], we reasoned that SREBP1c, the predominant isoform of SREBP1 in the liver[54], probably acts as a transcriptional regulator of miR-148a expression.

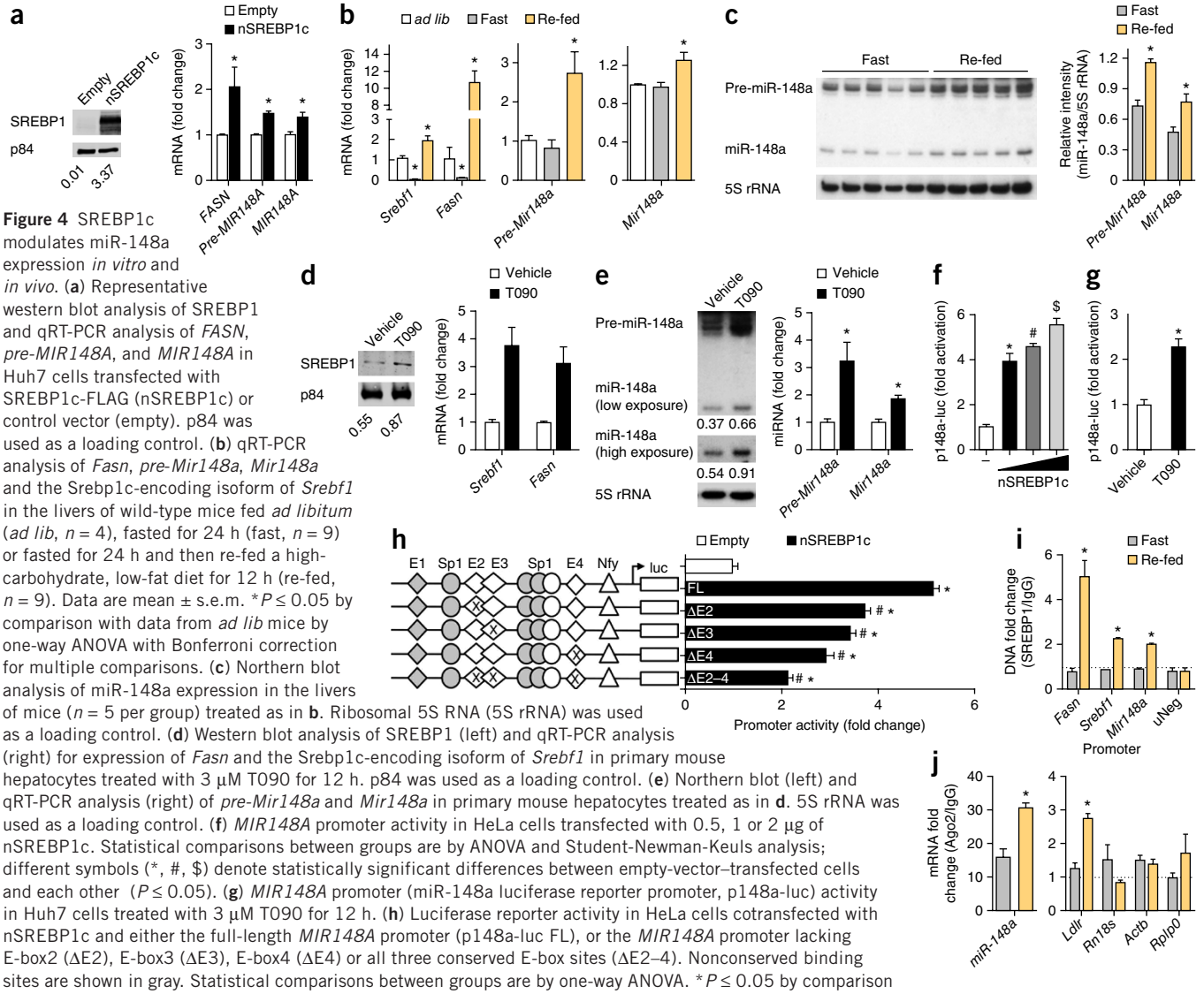

Figure 4 SREBP1c modulates miR-148a expression *in vitro* and *in vivo*. (**a**) Representative western blot analysis of SREBP1 and qRT-PCR analysis of *FASN*, *pre-MIR148A*, and *MIR148A* in Huh7 cells transfected with SREBP1c-FLAG (nSREBP1c) or control vector (empty). p84 was used as a loading control. (**b**) qRT-PCR analysis of *Fasn*, *pre-Mir148a*, *Mir148a* and the Srebp1c-encoding isoform of *Srebf1* in the livers of wild-type mice fed *ad libitum* (*ad lib*, $n = 4$), fasted for 24 h (fast, $n = 9$) or fasted for 24 h and then re-fed a high-carbohydrate, low-fat diet for 12 h (re-fed, $n = 9$). Data are mean ± s.e.m. $^{*}P \leq 0.05$ by comparison with data from *ad lib* mice by one-way ANOVA with Bonferroni correction for multiple comparisons. (**c**) Northern blot analysis of miR-148a expression in the livers of mice ($n = 5$ per group) treated as in **b**. Ribosomal 5S RNA (5S rRNA) was used as a loading control. (**d**) Western blot analysis of SREBP1 (left) and qRT-PCR analysis (right) for expression of *Fasn* and the Srebp1c-encoding isoform of *Srebf1* in primary mouse hepatocytes treated with 3 μM T090 for 12 h. p84 was used as a loading control. (**e**) Northern blot (left) and qRT-PCR analysis (right) of *pre-Mir148a* and *Mir148a* in primary mouse hepatocytes treated as in **d**. 5S rRNA was used as a loading control. (**f**) *MIR148A* promoter activity in HeLa cells transfected with 0.5, 1 or 2 μg of nSREBP1c. Statistical comparisons between groups are by ANOVA and Student-Newman-Keuls analysis; different symbols (*, #, $) denote statistically significant differences between empty-vector–transfected cells and each other ($P \leq 0.05$). (**g**) *MIR148A* promoter (miR-148a luciferase reporter promoter, p148a-luc) activity in Huh7 cells treated with 3 μM T090 for 12 h. (**h**) Luciferase reporter activity in HeLa cells cotransfected with nSREBP1c and either the full-length *MIR148A* promoter (p148a-luc FL), or the *MIR148A* promoter lacking E-box2 (ΔE2), E-box3 (ΔE3), E-box4 (ΔE4) or all three conserved E-box sites (ΔE2–4). Nonconserved binding sites are shown in gray. Statistical comparisons between groups are by one-way ANOVA. $^{*}P \leq 0.05$ by comparison with empty vector–transfected cells. $^{\#}P \leq 0.05$ by comparison with transfected with p148a-luc and nSREBP1. (**i**) Chromatin immunoprecipitation (ChIP) analysis of SREBP1 association with the *Fasn, Srebf1* and *Mir148a* promoters in the livers of mice ($n = 2$ or 3 pooled samples per group) treated as in **b**. An upstream region in the *Mir148a* promoter region that lacks predicted SREBP1-binding sites was used as a negative control (uNeg). (**j**) qRT-PCR analysis of *Mir148a* and *Ldlr* in the livers of mice treated as in **b** after Ago2 immunoprecipitation ($n \geq 2$ pooled samples per group). 18S (*Rn18s*), β-actin (*Actb*) and 36B4 (*Rplp0*) were used as negative controls. Relative expression levels were normalized to those in cells immunoprecipitated with a control IgG antibody (dashed line). Data are the mean ± s.e.m. and representative of ≥3 experiments in duplicate (**a**,**d**,**e**,**i**,**j**) or in triplicate (**f**–**h**). Relative intensities of the northern (**e**) and western blot bands (**a**,**d**) compared to the respective loading controls are shown below each blot. $^{*}P \leq 0.05$ compared to empty vector–containing cells (**a**), vehicle-treated cells (**d**,**e**,**g**) or fasting group (**c**,**i**,**j**) by unpaired *t*-test.

To test whether SREBP1c modulates miR-148a expression, we transfected Huh7 cells with a vector expressing FLAG-tagged nuclear SREBP1c (nSREBP1c) and measured miR-148a expression. Overexpression of nSREBP1c significantly increased the expression of *MIR148A* (both the precursor and mature forms) as well as that of the SREBP1c target gene *FASN* (**Fig. 4a**). To further explore the *in vivo* relevance of SREBP1c-dependent regulation of miR-148a, we measured levels of the mature form of miR-148a in the livers of mice that had been fasted for 24 h and subsequently re-fed a high-carbohydrate, low-fat diet for 12 h, a dietary condition that increases endogenous SREBP1c expression[55]. As expected, levels of both the precursor and the mature *Mir148a* paralleled the re-feeding–induced increase in mRNA levels of *Fasn* and the SREBP1c-encoding isoform of *Srebf1*, as assessed by qRT-PCR (**Fig. 4b**). We observed similar results for hepatic *pre-Mir148a* and *Mir148a* expression in fasted and re-fed mice by northern blotting (**Fig. 4c**).

LXR activates SREBP1c expression[56,57]. To ascertain whether miR-148a expression is regulated by LXR, we treated primary mouse hepatocytes and Huh7 cells with the synthetic LXR ligand T0901317 (T090) and measured miR-148a expression. LXR activation led to a significant upregulation of the expression of the mature SREBP1 protein as well as an increase in the mRNA levels of *Fasn*, the SREBP1c-encoding isoform of *Srebf1* (**Fig. 4d** and **Supplementary Fig. 6a**) and the precursor and mature forms of *Mir148a* (**Fig. 4e** and **Supplementary Fig. 6b**). To determine whether the induction of miR-148a expression by LXR is dependent on SREBP1c, we silenced *SREBF1* using RNA interference. The efficiency of siRNA knockdown was confirmed by qRT-PCR and western blotting (**Supplementary Fig. 6c**). After treatment with T090, *MIR148A* levels were markedly increased in cells that were treated with a control siRNA but not in those that were treated with a siRNA to *SREBF1* (**Supplementary Fig. 6d**,**e**), suggesting that SREBP1c is responsible for the induction of miR-148a expression by LXR.

We further investigated the role of SREBP1c in regulating miR-148a expression by generating luciferase reporter constructs containing

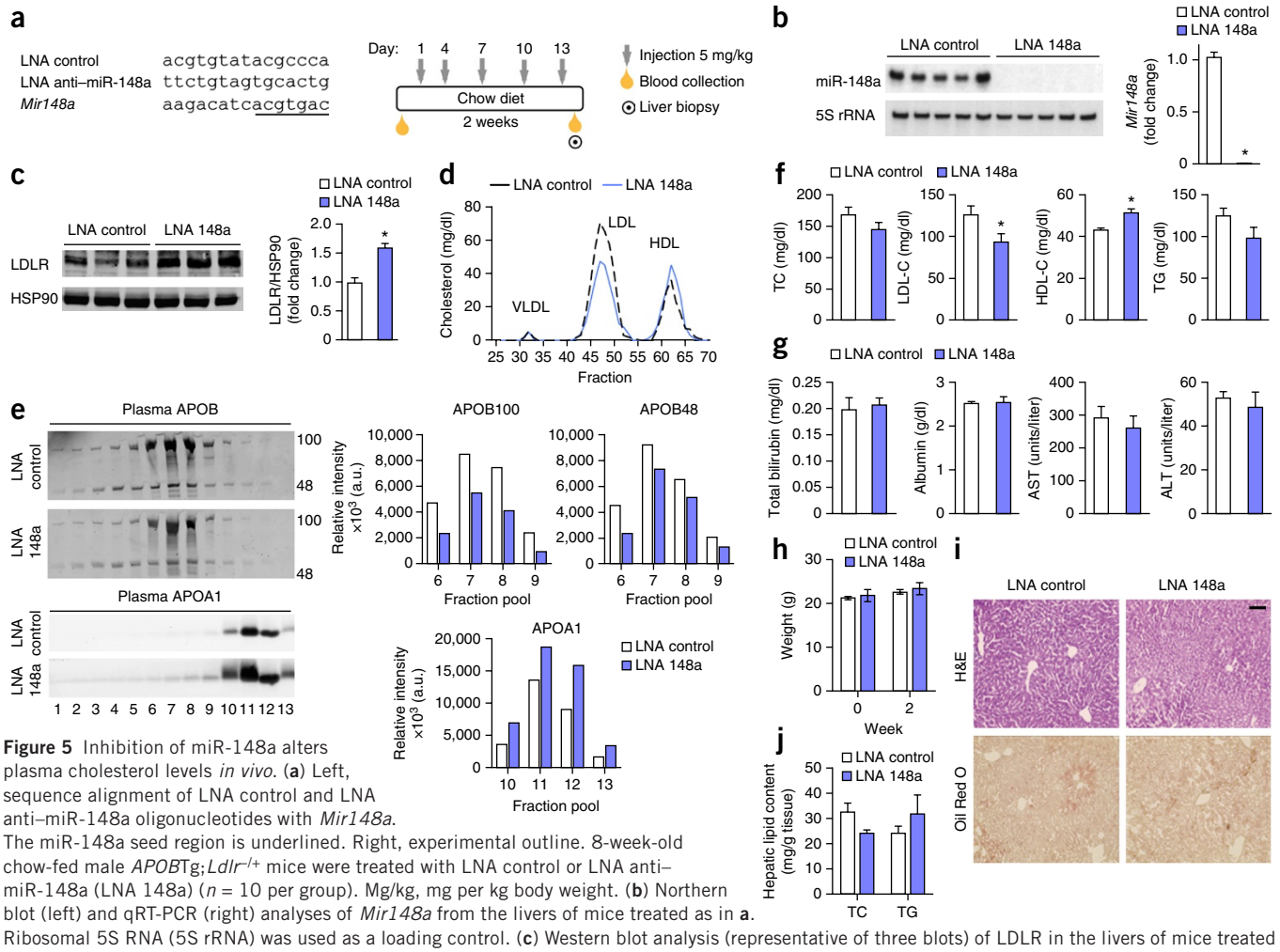

Figure 5 Inhibition of miR-148a alters plasma cholesterol levels *in vivo*. (**a**) Left, sequence alignment of LNA control and LNA anti–miR-148a oligonucleotides with *Mir148a*. The miR-148a seed region is underlined. Right, experimental outline. 8-week-old chow-fed male *APOB*Tg;*Ldlr*$^{-/+}$ mice were treated with LNA control or LNA anti–miR-148a (LNA 148a) ($n = 10$ per group). Mg/kg, mg per kg body weight. (**b**) Northern blot (left) and qRT-PCR (right) analyses of *Mir148a* from the livers of mice treated as in **a**. Ribosomal 5S RNA (5S rRNA) was used as a loading control. (**c**) Western blot analysis (representative of three blots) of LDLR in the livers of mice treated as in **a**. HSP90 was used as a loading control. (**d**) Cholesterol content of FPLC-fractionated lipoproteins from pooled plasma ($n = 5$ per group) of mice treated as in **a**. (**e**) Western blot analysis (representative of two blots) of plasma APOB and APOA1 in the FPLC-fractionated lipoproteins in panel **d**. Lanes 1–13 correspond to the following pooled fractions: 1 (28–30), 2 (31–33), 3 (34–36), 4 (37–39), 5 (40–42), 6 (43–45), 7 (46–48), 8 (49–51), 9 (52–54), 10 (55–57), 11 (58–60), 12 (61–63) and 13 (64–66). Relative intensities of APOB100, APOB48 and APOA1 are shown below. (**f**) Levels of total cholesterol (TC), LDL-C, HDL-C and triglycerides (TGs) in the plasma of mice ($n = 10$ mice per group) treated as in **a**. (**g**,**h**) Levels of total bilirubin, albumin, AST and ALT in plasma (**g**) and body weights (**h**) of mice treated with LNA control or LNA 148a ($n = 5$ per group). (**i**) Representative liver sections of mice ($n = 10$ per group) treated as in **a** and stained with H&E or Oil Red O. Scale bar, 70 µm. (**j**) TC and TGs in the livers of mice treated with LNA control or LNA 148a ($n = 5$ per group). All data are the mean ± s.e.m. *$P \leq 0.05$ by comparison with data from LNA control–treated mice by unpaired *t*-test (**b**,**c**,**f**). a.u., arbitrary units.

a 2.3-kb region of the human *MIR148A* promoter (p148a-lucFL). Overexpression of nSREBP1c increased *MIR148A* promoter activity as compared to that observed in cells transfected with an empty vector (**Fig. 4f**). In agreement with this result, LXR-mediated induction of endogenous SREBP1c by T090 also significantly increased *MIR148A* promoter activity (**Fig. 4g**), confirming that SREBP1c regulates *MIR148A* at the transcriptional level.

The promoter region of human *MIR148A* contains four E-box elements, three of which are conserved in mice (**Supplementary Fig. 5b**). To test which E-box elements are responsible for the SREBP1c-mediated induction of *MIR148A* transcription, we designed miR-148a promoter constructs with deletions of each of the three conserved E-box motifs (herein named E-box2, E-box3 and E-box4, respectively). Deletion of each of these E-boxes significantly attenuated SREBP1c-dependent promoter activity (**Fig. 4h**). Moreover, when all three conserved E-box elements were simultaneously deleted, miR-148a reporter activity was further diminished upon nSREBP1c overexpression, suggesting that SREBP1c acts through E-box2, E-box3 and E-box4 to fully induce *MIR148A* transcription. Indeed, when we transfected cells with a shortened promoter construct (p148a-lucT) lacking the nonconserved E-box1 motif, *MIR148A* promoter activity was unaffected (**Supplementary Fig. 6f**).

Finally, to assess whether Srebp1 binds directly to the *Mir148a* promoter, we performed ChIP assays from the livers of mice that were fasted for 24 h or that had been fasted for 24 h and subsequently re-fed a high-carbohydrate, low-fat diet for 12 h (**Fig. 4i**). We found that Srebp1 was significantly enriched in the promoters of *Srebf1*, *Fasn* and *Mir148a* upon re-feeding. Notably, no Srebp1 enrichment was observed in an upstream region of the *Mir148a* promoter that lacks Srebp1-binding sites (uNeg). Moreover, we found an enrichment of *Mir148a* and *Ldlr* mRNAs in RISC complexes from the livers of mice that had been fasted and subsequently re-fed (**Fig. 4j**). Altogether, these results provide compelling evidence that Srebp1c directly regulates the transcriptional expression of the *Mir148a* gene by binding to the E-box2, E-box3 and E-box4 elements and that Srebp1c controls miR-148a expression *in vivo*.

Modulation of miR-148a expression alters plasma lipids *in vivo*

In light of the role of miR-148a in negatively regulating LDLR expression and activity *in vitro*, we next assessed the functional effects of inhibiting miR-148a *in vivo*. Because the rate of hepatic LDL clearance is 40-fold greater in wild-type C57BL/6 mice than in humans[58], we used for our studies mice that express a human apolipoprotein B (*APOB*) transgene (which encodes the APOB100 isoform) in an *Ldlr* heterozygote background (*APOB*Tg;*Ldlr*$^{-/+}$) and thus display an LDL- and HDL-dominant lipoprotein profile (**Supplementary Fig. 7**). To inhibit miR-148a expression, male *APOB*Tg;*Ldlr*$^{-/+}$ mice were injected every 3 d for a period of 2 weeks with 5 mg per kg of body weight (mg/kg) of locked nucleic acid (LNA) antisense oligonucleotides targeting miR-148a (LNA 148a) (**Fig. 5a**). A scrambled LNA oligonucleotide was used as a control (LNA control). Twenty-four hours after the last injection, the mice were killed and the sera and livers were collected for plasma cholesterol and gene expression analysis, respectively. Treatment with LNA 148a markedly decreased the levels of hepatic *Mir148a* (**Fig. 5b**) and significantly increased hepatic LDLR expression (**Fig. 5c**) as compared to that in controls. Consistent with these results, fractionation of plasma lipoproteins revealed a marked decrease in LDL-C levels in *APOB*Tg;*Ldlr*$^{-/+}$ mice treated with LNA 148a (**Fig. 5d–f**). Notably, inhibition of miR-148a also significantly increased HDL-C levels (**Fig. 5d**,**f**). As expected by the significant

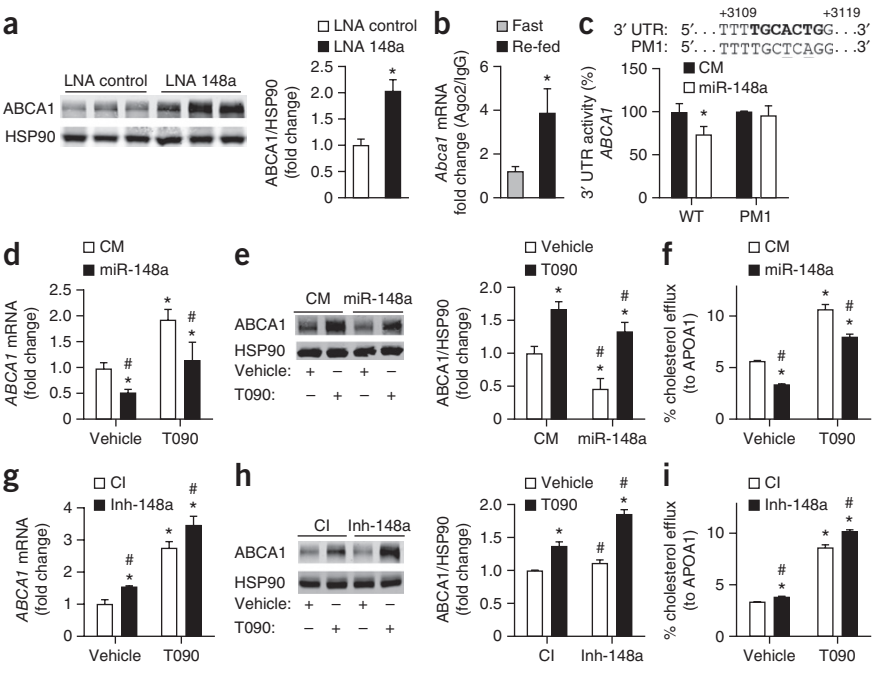

Figure 6 miR-148a post-transcriptionally regulates *ABCA1* expression. (**a**) Western blot analysis (representative of three blots) of ABCA1 expression in the livers of mice treated as in **Figure 5a**. HSP90 was used as a loading control. $^{*}P \leq 0.05$ by comparison with data from LNA control–treated mice by unpaired *t*-test. (**b**) qRT-PCR analysis of *Abca1* after Ago2 immunoprecipitation from the livers of mice that were fasted with or without re-feeding, as in **Figure 4j** ($n = \geq 2$ samples per group). $^{*}P \leq 0.05$ by comparison with data from fasted mice by unpaired *t*-test. (**c**) Top, predicted miR-148a binding site (bold) at position 3112–3118 of the *ABCA1* 3′ UTR. Point mutations (PM1) introduced into the binding site are underlined. Bottom, luciferase reporter activity in COS7 cells transfected with a control mimic (CM) or miR-148a mimic (miR-148a) and a reporter construct containing WT or mutated versions of the 3′ UTR of the human *ABCA1* gene. $^{*}P \leq 0.05$ compared to CM-transfected cells by unpaired *t*-test. (**d**,**e**) qRT-PCR (**d**) and western blot (**e**) analysis of *ABCA1* expression in Huh7 cells transfected with CM or miR-148a in the absence or presence of T090. HSP90 was used as a loading control. (**f**) Cholesterol efflux to APOA1 in Huh7 cells treated as in **d**. (**g**,**h**) qRT-PCR (**g**) and western blot (**h**) analysis of ABCA1 expression in Huh7 cells transfected with a control inhibitor (CI) or Inh-148a in the absence or presence of T090. HSP90 was used as a loading control. (**i**) Cholesterol efflux to APOA1 in Huh7 cells treated as in **g**. Data are the mean ± s.e.m. and representative of ≥3 experiments in triplicate. Statistical comparisons between groups by one-way ANOVA with Bonferroni correction for multiple comparisons (**d**–**i**); $^{*}P \leq 0.05$ by comparison with data from cells transfected with CM or CI in vehicle-treated cells; $^{\#}P \leq 0.05$ by comparison with data from cells transfected with CM or CI in T090-treated cells.

decrease in the LDL-C and increase in the HDL-C fractions, the expression of APOB100 and APOA1 was diminished and enhanced, respectively, in pooled plasma samples isolated from mice treated with LNA 148a as compared to those in the controls (**Fig. 5e**). Similar effects on plasma lipoprotein distribution and apolipoprotein expression were observed in a separate cohort of mice (**Supplementary Fig. 8a–c**). Total plasma cholesterol levels were slightly, but not significantly, decreased in mice treated with LNA anti-miR-148a (**Fig. 5f**), consistent with the finding that miR-148a antagonism has opposing effects on LDL-C and HDL-C. LDL-C levels in *Ldlr*$^{-/-}$ mice were unaffected by LNA 148a treatment (**Supplementary Fig. 9**), indicating that the effect of miR-148a on LDL-C levels is mediated by the LDLR. The effects of LNA 148a on lipoprotein metabolism were not influenced by liver toxicity, as indicated by similar blood levels of alanine transaminase (ALT), asparagine transaminase (AST), albumin and total bilirubin in LNA 148a– and LNA control–treated mice (**Fig. 5g**). Moreover, *Mir148a* silencing did not affect body weight (**Fig. 5h**) or hepatic lipid accumulation (**Fig. 5i**,**j**).

The impact of anti-miR-148a treatment on lipoprotein metabolism was confirmed in *APOB*Tg;*Ldlr*$^{-/+}$ mice fed an HFD for 1 month (**Supplementary Fig. 10a–c**). Similarly to the results in chow diet–fed mice (**Fig. 5c**), HFD-fed mice treated with LNA 148a had increased levels of hepatic LDLR (**Supplementary Fig. 10d**), a marked decrease in LDL-C and a marked increase in HDL-C levels (**Supplementary Fig. 10f**,**g**). LNA 148a treatment did not affect body weight or hepatic lipids (**Supplementary Fig. 10h–j**).

To gain a better understanding of how miR-148a might regulate HDL-C levels *in vivo*, we analyzed additional predicted miR-148a target genes. Of note, we found a conserved predicted miR-148a–binding site within the 3′ UTR of *ABCA1* (**Supplementary Fig. 3a**,**c**). Given that ABCA1 has a major role in regulating HDL biogenesis in the liver[59], we hypothesized that the increased HDL-C levels observed in LNA 148a–treated mice is due to miR-148a–mediated regulation of ABCA1. Indeed, we found a substantial increase in hepatic ABCA1 protein levels in LNA 148a–treated mice as compared to that in controls (**Fig. 6a**; **Supplementary Fig. 10e**).

miR-148a directly targets the 3′ UTR of *ABCA1*

To assess whether miR-148a targets *Abca1*, we first performed ribonucleoprotein immunoprecipitation (RNP-IP) using an Ago2-specific antibody from the livers of mice that were fasted or that had been fasted and then re-fed a high-carbohydrate diet, a condition that enriches miR-148a in the RISC complex (**Fig. 4j**). Re-feeding significantly enriched the association of *Abca1* mRNA in Ago2-containing complexes (**Fig. 6b**), suggesting that miR-148a regulates ABCA1 under physiological conditions. Luciferase reporter assays revealed a significant downregulation of human *ABCA1* 3′ UTR activity in cells transfected with a miR-148a mimic, as compared to control cells (**Fig. 6c**). Of note, specific point mutations in the predicted miR-148a–binding site (PM1) abolished the inhibitory effect of miR-148a on *ABCA1* 3′ UTR activity (**Fig. 6c**). To determine whether miR-148a regulates ABCA1 expression and cholesterol efflux in human hepatic cells, we transfected Huh7 cells with a miR-148a mimic or inhibitor. miR-148a overexpression strongly reduced *ABCA1* mRNA and protein levels under both basal conditions (vehicle) and after treatment with T090 to directly stimulate LXR-dependent ABCA1 expression (**Fig. 6d**,**e**), and it also significantly attenuated cholesterol efflux to APOA1 (**Fig. 6f**). Inhibition of endogenous miR-148a in Huh7 cells increased *ABCA1* mRNA and protein levels and resulted in elevated cholesterol efflux to APOA1 (**Fig. 6g–i**). Taken together, these experiments identify ABCA1 as a direct target of miR-148a.

DISCUSSION

Our data support the importance of miRNAs in contributing to the regulatory circuitry of cholesterol metabolism, particularly with respect to the SREBPs. Notably, the role of miR-33a and miR-33b (miR-33a/b) in controlling lipid homeostasis has been extensively studied. miR-33a and miR-33b are located within the introns of the *SREBF2* and *SREBF1* genes, respectively. Both miR-33a and miR-33b are cotranscribed with their host genes under conditions that increase SREBP activation and act to control cholesterol and fatty acid homeostasis by targeting genes involved in cellular cholesterol efflux and fatty acid oxidation. Moreover, miR-185 was recently shown to regulate cholesterol homeostasis in concert with the genes encoding the SREBPs. In particular, miR-185 is transcriptionally activated by SREBP1c and negatively regulates SREBP2 expression, thereby inhibiting *de novo* cholesterol biosynthesis and LDL uptake[60]. Here we show that miR-148a directly controls LDLR activity and is transcriptionally activated by SREBP1c *in vitro* and *in vivo*. Similarly to miR-185, LXR-mediated induction of SREBP1c results in increased expression of miR-148a. These results suggest that LDLR expression is regulated by the SREBP1c-dependent induction of miR-148a; however, we cannot rule out the possibility that the LXR-mediated decrease in LDLR expression could also be due to an increase in miR-185 or IDOL expression. Given that IDOL is not highly expressed in mouse liver, further studies in nonhuman primates are needed to assess the physiologic contribution of each pathway to the post-transcriptional regulation of hepatic LDLR expression in humans.

In addition to miR-33 and miR-185, the locus comprising miR-96, miR-182 and miR-183 (miR-96/182/183) also acts in a feedback loop to regulate cholesterol metabolism. This locus is directly regulated by SREBP2 and regulates activation of SREBP2 by controlling its processing (via targeting of insulin-induced gene 2 (INSIG2)) and stability (via targeting of F-box and WD repeat domain containing 7 (FBXW7)) in cultured cells[18]. Of note, antagonism of miR-182 in mice had no significant effect on circulating cholesterol and triglyceride levels. Because these studies were conducted in wild-type mice, which have an HDL-dominant lipoprotein profile, future studies using 'humanized' mouse models may yield alternative results.

For our *in vivo* analysis, we employed the *APOB*Tg;*Ldlr*$^{-/+}$ mouse model, which displays an LDL-dominant lipoprotein profile, and found a significant decrease in LDL-C when hepatic miR-148a levels were antagonized. As a major route for the clearance of APOE- and APOB-containing lipoproteins is LDLR-mediated endocytosis in the liver[58], the reduction in LDL-C by miR-148a antagonism is likely to be due mainly to miR-148a–mediated repression of hepatic LDLR expression. Although the possibility exists that miR-148a affects other pathways that control lipid metabolism, our data unequivocally establish a key role for miR-148a in regulating LDLR activity *in vivo*. We also provide evidence that miR-148a post-transcriptionally controls hepatic ABCA1 expression and cellular cholesterol efflux to APOA1, such that antagonism of miR-148a significantly increases circulating HDL-C levels *in vivo*.

Human genetic data suggests that miR-148a has a role predominantly in governing LDL-C metabolism, as a SNP (rs4722551) in the *MIR148A* promoter region is strongly associated with altered LDL-C levels in humans[37–39]. Here we provide insight into the mechanism by which this variant might alter plasma LDL-C levels: by affecting

transcriptional activation of *MIR148A* and, consequently, LDLR expression. Future experiments are warranted to dissect the contribution of this variant to altered lipid levels and cardiovascular disease risk.

In conclusion, our results underscore the importance of miRNAs in the post-transcriptional regulation of LDLR activity. Specifically, because suppression of miR-148a activity simultaneously reduces LDL-C and increases HDL-C concentrations, our data highlight the therapeutic potential of this approach for the treatment of atherosclerosis and related dyslipidemias.

METHODS

Methods and any associated references are available in the online version of the paper.

Note: Any Supplementary Information and Source Data files are available in the online version of the paper.

ACKNOWLEDGMENTS

We thank C. Yun, J. Recio, S. Katz and R. DasGupta at the New York University (NYU) RNAi Core for their advice and assistance with the miRNA screen, K. Harry and members of the Yale University Liver Center for primary mouse hepatocyte isolation, members of the Iwakiri laboratory for reagents and advice on primary hepatocyte culture, the Yale University School of Medicine Mouse Metabolic Phenotyping Center (MMPC) for liver toxicity measurements, P. Tontonoz (UCLA) for generously providing the LDLR-GFP plasmid, the Nonhuman Primate Core of the National Institute on Aging for providing liver samples and E. Fisher (NYU School of Medicine) for kindly providing the human hepatocellular carcinoma cell line (Huh7) and mouse hepatic cell line (Hepa1–6). This work was supported through grants by the US National Institutes of Health (NIH; grants R01HL107953, R01HL107953-04S1 and R01HL106063 (C.F.-H.); grant R01HL105945 (Y.S.); grant 1F31AG043318 (L.G.); grant P30KD034989 (Yale University Liver Center), the American Heart Association (grant 15SDG23000025 (C.M.R.)), the Howard Hughes Medical Institute International Student Research Fellowship (E.A.), the Foundation Leducq Transatlantic Network of Excellence in Cardiovascular Research (C.F.-H.) and the Ministerio de Industria y Comercio, Spain (grant SAF2011-29951 (M.A.L.)). Centro de Investigación Biomédica en Red Fisiopatología de Obesidad y Nutrición (CIBERobn) is an initiative of Instituto de Salud Carlos III (ISCIII), Spain. R.d.C. is supported by the Intramural Research Program of the NIH, National Institute of Aging. A.M.N. and A.W. are supported by NIH grant R01DK 094184. The NYU RNAi core is supported by the Laura and Isaac Perlmutter Cancer Center (NIH, National Cancer Institute grant P30CA16087) and the New York State Stem Cell Science (NYSTEM) contract C026719. The Yale University School of Medicine MMPC is supported by NIH grant U24 DK059635.

AUTHOR CONTRIBUTIONS

L.G. and C.F.-H. conceived and designed the study. L.G. optimized and performed the miRNA screen. J.F.A. and A.C.-D. performed confocal experiments, assisted with cloning and analyzed data. L.G. and A.C.-D. performed *in vitro* experiments and analyzed data. L.G., N.R., C.M.R. and A.C.-D. performed mouse experiments and analyzed data. N.R. performed western blotting for plasma lipoproteins and assessed lipoprotein distribution by FPLC. E.A. cloned the *MIR148A* promoter. C.-S.L. assisted with western blotting. N.N.A. analyzed gene expression in the livers of fed and fasted wild-type mice and *ob*/*ob* mice. R.d.C. designed the nonhuman primate experiments and J.D.H. provided the mouse samples. M.A.L. provided DiI-LDL and native LDL. A.W. and A.M.N. assisted with mouse experiments. Y.S. and C.F.-H. assisted with experimental design and data interpretation. L.G. and C.F.-H. wrote the manuscript, which was commented on by all authors.

COMPETING FINANCIAL INTERESTS

The authors declare competing financial interests: details are available in the online version of the paper.

1. Glass, C.K. & Witztum, J.L. Atherosclerosis. the road ahead. *Cell* **104**, 503–516 (2001).
2. Lusis, A.J. Atherosclerosis. *Nature* **407**, 233–241 (2000).
3. Brown, M.S. & Goldstein, J.L. The SREBP pathway: regulation of cholesterol metabolism by proteolysis of a membrane-bound transcription factor. *Cell* **89**, 331–340 (1997).
4. Zelcer, N., Hong, C., Boyadjian, R. & Tontonoz, P. LXR regulates cholesterol uptake through Idol-dependent ubiquitination of the LDL receptor. *Science* **325**, 100–104 (2009).
5. Hua, X. *et al.* SREBP-2, a second basic-helix-loop-helix–leucine zipper protein that stimulates transcription by binding to a sterol regulatory element. *Proc. Natl. Acad. Sci. USA* **90**, 11603–11607 (1993).
6. Tontonoz, P., Kim, J.B., Graves, R.A. & Spiegelman, B.M. ADD1: a novel helix-loop-helix transcription factor associated with adipocyte determination and differentiation. *Mol. Cell. Biol.* **13**, 4753–4759 (1993).
7. Yokoyama, C. *et al.* SREBP-1, a basic-helix-loop-helix–leucine zipper protein that controls transcription of the low density lipoprotein receptor gene. *Cell* **75**, 187–197 (1993).
8. Goldstein, J.L. & Brown, M.S. Regulation of the mevalonate pathway. *Nature* **343**, 425–430 (1990).
9. Walker, A.K. *et al.* A conserved SREBP-1–phosphatidylcholine feedback circuit regulates lipogenesis in metazoans. *Cell* **147**, 840–852 (2011).
10. Horton, J.D. *et al.* Combined analysis of oligonucleotide microarray data from transgenic and knockout mice identifies direct SREBP target genes. *Proc. Natl. Acad. Sci. USA* **100**, 12027–12032 (2003).
11. Maxwell, K.N., Soccio, R.E., Duncan, E.M., Sehayek, E. & Breslow, J.L. Novel putative SREBP and LXR target genes identified by microarray analysis in liver of cholesterol-fed mice. *J. Lipid Res.* **44**, 2109–2119 (2003).
12. Beaven, S.W. & Tontonoz, P. Nuclear receptors in lipid metabolism: targeting the heart of dyslipidemia. *Annu. Rev. Med.* **57**, 313–329 (2006).
13. Ambros, V. The functions of animal microRNAs. *Nature* **431**, 350–355 (2004).
14. Bartel, D.P. MicroRNAs: target recognition and regulatory functions. *Cell* **136**, 215–233 (2009).
15. Filipowicz, W., Bhattacharyya, S.N. & Sonenberg, N. Mechanisms of post-transcriptional regulation by microRNAs: are the answers in sight? *Nat. Rev. Genet.* **9**, 102–114 (2008).
16. Rayner, K.J. *et al.* MiR-33 contributes to the regulation of cholesterol homeostasis. *Science* **328**, 1570–1573 (2010).
17. Najafi-Shoushtari, S.H. *et al.* MicroRNA-33 and the SREBP host genes cooperate to control cholesterol homeostasis. *Science* **328**, 1566–1569 (2010).
18. Jeon, T.I. *et al.* An SREBP-responsive microRNA operon contributes to a regulatory loop for intracellular lipid homeostasis. *Cell Metab.* **18**, 51–61 (2013).
19. Rayner, K.J. *et al.* Antagonism of miR-33 in mice promotes reverse cholesterol transport and regression of atherosclerosis. *J. Clin. Invest.* **121**, 2921–2931 (2011).
20. Rayner, K.J. *et al.* Inhibition of miR-33a/b in nonhuman primates raises plasma HDL and lowers VLDL triglycerides. *Nature* **478**, 404–407 (2011).
21. Rottiers, V. *et al.* Pharmacological inhibition of a microRNA family in nonhuman primates by a seed-targeting 8-mer antimiR. *Sci. Transl. Med.* **5**, 212ra162 (2013).
22. de Aguiar Vallim, T.Q. *et al.* MicroRNA-144 regulates hepatic *ABCA1* and plasma HDL following activation of the nuclear receptor FXR. *Circ. Res.* **112**, 1602–1612 (2013).
23. Ramírez, C.M. *et al.* Control of cholesterol metabolism and plasma HDL levels by miRNA-144. *Circ. Res.* **112**, 1592–1601 (2013).
24. Vickers, K.C. *et al.* MicroRNA-223 coordinates cholesterol homeostasis. *Proc. Natl. Acad. Sci. USA* **111**, 14518–14523 (2014).
25. Elmén, J. *et al.* LNA-mediated microRNA silencing in nonhuman primates. *Nature* **452**, 896–899 (2008).
26. Elmén, J. *et al.* Antagonism of microRNA-122 in mice by systemically administered LNA-antimiR leads to upregulation of a large set of predicted target mRNAs in the liver. *Nucleic Acids Res.* **36**, 1153–1162 (2008).
27. Esau, C. *et al.* miR-122 regulation of lipid metabolism revealed by *in vivo* antisense targeting. *Cell Metab.* **3**, 87–98 (2006).
28. Soh, J., Iqbal, J., Queiroz, J., Fernandez-Hernando, C. & Hussain, M.M. MicroRNA-30c reduces hyperlipidemia and atherosclerosis in mice by decreasing lipid synthesis and lipoprotein secretion. *Nat. Med.* **19**, 892–900 (2013).
29. Brown, M.S., Dana, S.E. & Goldstein, J.L. Regulation of 3-hydroxy-3-methylglutaryl coenzyme A reductase activity in human fibroblasts by lipoproteins. *Proc. Natl. Acad. Sci. USA* **70**, 2162–2166 (1973).
30. Goldstein, J.L., Basu, S.K., Brunschede, G.Y. & Brown, M.S. Release of low-density lipoprotein from its cell surface receptor by sulfated glycosaminoglycans. *Cell* **7**, 85–95 (1976).
31. Zhang, J.H., Chung, T.D. & Oldenburg, K.R. A simple statistical parameter for use in evaluation and validation of high-throughput screening assays. *J. Biomol. Screen.* **4**, 67–73 (1999).
32. Birmingham, A. *et al.* Statistical methods for analysis of high-throughput RNA interference screens. *Nat. Methods* **6**, 569–575 (2009).
33. Barad, O. *et al.* MicroRNA expression detected by oligonucleotide microarrays: system establishment and expression profiling in human tissues. *Genome Res.* **14**, 2486–2494 (2004).
34. Landgraf, P. *et al.* A mammalian microRNA expression atlas based on small RNA library sequencing. *Cell* **129**, 1401–1414 (2007).
35. Vickers, K.C. *et al.* MicroRNA-27b is a regulatory hub in lipid metabolism and is altered in dyslipidemia. *Hepatology* **57**, 533–542 (2013).
36. Arora, A. & Simpson, D.A. Individual mRNA expression profiles reveal the effects of specific microRNAs. *Genome Biol.* **9**, R82 (2008).
37. Do, R. *et al.* Common variants associated with plasma triglycerides and risk for coronary artery disease. *Nat. Genet.* **45**, 1345–1352 (2013).

38. Global Lipids Genetics Consortium. *et al.* Discovery and refinement of loci associated with lipid levels. *Nat. Genet.* **45**, 1274–1283 (2013).
39. Huan, T. *et al.* Genome-wide identification of microRNA expression quantitative trait loci. *Nat. Commun.* **6**, 6601 (2015).
40. Trajkovski, M. *et al.* MicroRNAs 103 and 107 regulate insulin sensitivity. *Nature* **474**, 649–653 (2011).
41. Mercer, J. *et al.* RNAi screening reveals proteasome- and Cullin3-dependent stages in vaccinia virus infection. *Cell Rep.* **2**, 1036–1047 (2012).
42. John, B. *et al.* Human MicroRNA targets. *PLoS Biol.* **2**, e363 (2004).
43. Lewis, B.P., Burge, C.B. & Bartel, D.P. Conserved seed pairing, often flanked by adenosines, indicates that thousands of human genes are microRNA targets. *Cell* **120**, 15–20 (2005).
44. Dweep, H., Gretz, N. & Sticht, C. miRWalk database for miRNA-target interactions. *Methods Mol. Biol.* **1182**, 289–305 (2014).
45. Huang, D.W., Sherman, B.T. & Lempicki, R.A. Systematic and integrative analysis of large gene lists using DAVID bioinformatics resources. *Nat. Protoc.* **4**, 44–57 (2009).
46. Szklarczyk, D. *et al.* The STRING database in 2011: functional interaction networks of proteins, globally integrated and scored. *Nucleic Acids Res.* **39**, D561–D568 (2011).
47. Thomas, P.D. *et al.* PANTHER: a library of protein families and subfamilies indexed by function. *Genome Res.* **13**, 2129–2141 (2003).
48. Down, T.A. & Hubbard, T.J. Computational detection and location of transcription start sites in mammalian genomic DNA. *Genome Res.* **12**, 458–461 (2002).
49. Saini, H.K., Griffiths-Jones, S. & Enright, A.J. Genomic analysis of human microRNA transcripts. *Proc. Natl. Acad. Sci. USA* **104**, 17719–17724 (2007).
50. Ernst, J. & Kellis, M. Discovery and characterization of chromatin states for systematic annotation of the human genome. *Nat. Biotechnol.* **28**, 817–825 (2010).
51. Ernst, J. *et al.* Mapping and analysis of chromatin state dynamics in nine human cell types. *Nature* **473**, 43–49 (2011).
52. Kent, W.J. *et al.* The human genome browser at UCSC. *Genome Res.* **12**, 996–1006 (2002).
53. Shimomura, I., Bashmakov, Y. & Horton, J.D. Increased levels of nuclear SREBP-1c associated with fatty livers in two mouse models of diabetes mellitus. *J. Biol. Chem.* **274**, 30028–30032 (1999).
54. Shimomura, I., Shimano, H., Horton, J.D., Goldstein, J.L. & Brown, M.S. Differential expression of exons 1a and 1c in mRNAs for sterol regulatory element binding protein-1 in human and mouse organs and cultured cells. *J. Clin. Invest.* **99**, 838–845 (1997).
55. Horton, J.D., Bashmakov, Y., Shimomura, I. & Shimano, H. Regulation of sterol regulatory element binding proteins in livers of fasted and refed mice. *Proc. Natl. Acad. Sci. USA* **95**, 5987–5992 (1998).
56. Peet, D.J. *et al.* Cholesterol and bile acid metabolism are impaired in mice lacking the nuclear oxysterol receptor LXR alpha. *Cell* **93**, 693–704 (1998).
57. Yoshikawa, T. *et al.* Identification of liver X receptor-retinoid X receptor as an activator of the sterol regulatory element-binding protein 1c gene promoter. *Mol. Cell. Biol.* **21**, 2991–3000 (2001).
58. Dietschy, J.M., Turley, S.D. & Spady, D.K. Role of liver in the maintenance of cholesterol and low density lipoprotein homeostasis in different animal species, including humans. *J. Lipid Res.* **34**, 1637–1659 (1993).
59. Oram, J.F. & Vaughan, A.M. ABCA1-mediated transport of cellular cholesterol and phospholipids to HDL apolipoproteins. *Curr. Opin. Lipidol.* **11**, 253–260 (2000).
60. Yang, M. *et al.* Identification of miR-185 as a regulator of *de novo* cholesterol biosynthesis and low density lipoprotein uptake. *J. Lipid Res.* **55**, 226–238 (2014).

ONLINE METHODS

Materials. For the LDLR-GFP plasmid, human LDLR cDNA was cloned into the pEGFP-N3 vector (Clontech). The pcDNA3.1-2×FLAG-SREBP1c vector (#26802) and empty control vector were from Addgene. Chemicals were obtained from Sigma-Aldrich unless otherwise noted. The synthetic LXR ligand T0901317 (T090) was purchased from Cayman Chemical. Human APOA1 was obtained from Meridian Life Sciences. Lipoprotein-deficient serum (LPDS) was prepared from FBS delipidated with 4% fumed silica. 1,1′-dioctadecyl-3,3,3,3′-tetramethylindocarbocyanineperclorate (DiI) was purchased from Molecular Probes (Invitrogen). Mouse monoclonal antibodies against ABCA1 (#ab18180) and APOA1 (#ab20453) were purchased from Abcam. Rabbit polyclonal antibodies against LDLR (#1007665) and SREBP1 (clone C-20, #sc-366) were from Cayman Chemical and Santa Cruz, respectively. Mouse monoclonal antibodies against HSP90 (#610418) and p84 (clone 5E10, #GTX70220) were purchased from BD Bioscience and GeneTex. Mouse monoclonal antibodies against LDLR (clone C7, #sc-18823) and SREBP1 (clone 2A4, #NB600-582) were obtained from Santa Cruz and Novus, respectively. Normal IgG (#2729) and ChIP-grade rabbit polyclonal antibodies against SREBP1 (clone H-160, #sc-8984X) were purchased from Cell Signaling and Santa Cruz, respectively. A mouse monoclonal antibody against APOB (#K23300R) was purchased from Meridian Life Sciences. A mouse monoclonal antibody against AGO2 (clone 2D4, #014-22023) was purchased from Wako Chemicals. Secondary fluorescently labeled antibodies were from Molecular Probes (Invitrogen). miRNA mimics and inhibitors were obtained from Dharamcon. A scrambled miR-148a mimic (CM*) was designed and purchased from Dharmacon. siRNAs were purchased from Dharmacon and locked nucleic acid (LNA) miRNA detection probes were purchased from Exiqon (Woburn, MA). For *in vivo* experiments, miRCURY locked nucleic acid (LNA) miRNA inhibitors targeting mature *Mir148a* or a scrambled control was purchased from Exiqon.

Cell culture. Human (HepG2) hepatic cells, monkey kidney fibroblast (COS7) cells and human cervical cancer (HeLa) cells were obtained from the American Type Culture Collection (ATCC). Huh7, HepG2, Hepa1–6 (Hepa), HeLa and COS7 cells were maintained in Dulbecco's Modified Eagle Medium (DMEM) containing 10% FBS (FBS) and 2% penicillin-streptomycin in 10 cm^2 dishes at 37 °C and 5% CO_2. Before experiments were performed, all cell lines were tested for mycoplasma contamination by PCR. For DiI-LDL uptake and binding experiments, cells were cultured in DMEM containing 10% LPDS and incubated with 30 μg/ml DiI-LDL cholesterol.

miRNA screen. All steps of the genome-wide miRNA screen, including reverse transfection and image acquisition and analysis, were performed at the New York University (NYU) RNAi Core Facility (NYU School of Medicine).

Reverse transfection, fixation and staining. Huh7 cells were reverse-transfected in triplicate with a library of 1,719 miRNA mimics (Life Technologies *mir*Vana Mimic Library, miRBase release 17.0) in Corning 384-well flat clear-bottom black plates (Fisher Scientific) using a standard reverse transfection protocol. Briefly, Huh7 cells (5,000 cells/well in 30 μl of DMEM media containing 10% LPDS) were seeded into a well containing 30 μl of transfection mix (25 μl of Optimem, 0.07 μl RNAi Max (Invitrogen) and 5 μl of 0.3 μM miRNA or control siRNA). 20 μl of fresh LPDS media was added to all wells 12 h post transfection, giving a final mimic concentration of 18 nM. 48 h later, cells were incubated with 10 μl of fresh LPDS containing 30 μg of DiI–LDL-C/ml for 8 h at 37 °C. Following incubation, cells were washed twice with 1× PBS and fixed with 4% PFA for 15 min. After three subsequent washes with 1× PBS, cells were incubated with PBS containing 1 μg/ml Hoechst (Molecular Probes) for 25 min, washed once with 1× PBS, spun down and imaged with an automated microscope. All liquid handling steps, including seeding, DiI-LDL incubation, fixation, washing and Hoechst incubation were performed using a Wellmate Microplate Dispenser (Matrix Technologies) and a BioTek plate washer (PerkinElmer). The triplicate screen consisted of 15 384-well plates and was completed over the course of 4 d.

Image acquisition and analysis. Automated high-content and high-throughput images were acquired using an Arrayscan VTI HCS Reader (Thermo Scientific) with a Zeiss 10× objective. 384-well plates were loaded onto the microscope using a Catalyst Express robotic arm and imaged overnight. In each well, cell nuclei and DiI-LDL intensities were imaged in five predefined fields. Image data was analyzed using BioApplication's Target Activation V3 image analysis software (Thermo Scientific). Briefly, nuclei were first identified on the Hoechst stain (channel 1). Following this, cell boundaries were estimated using the geometric segmentation method and used to calculate DiI intensity (channel 2) within each cell. Valid object count, mean average intensity and total average intensity of DiI were recorded for each field. For the primary screen, 57,600 images, consisting of an average of 533,528 objects/plate, were analyzed.

Hit classification. miRNAs were scored on their ability to significantly increase or decrease DiI intensity as compared to that of negative controls. Cytotoxic miRNA overexpression phenotypes were filtered for hit classification by excluding wells in which fewer than 500 cells were identified as valid objects. In addition, 32 validated internal controls, including nonsilencing (NS) siRNAs and siRNAs against LDLR (**Fig. 1**), as well as nontargeting negative-control miRNAs (control mimics) and siRNAs targeting *KIF11* (Life Technologies), were used on each plate to monitor transfection efficiency. After confirming efficient transfection efficiency, mean average intensities of each well were normalized to plate medians and converted to robust *z*-scores using Matlab, as previously described[32]. Robust *z*-scores were compared between each plate replicate and the mean of each score was calculated and used to rank potential candidates. Those miRNAs that had a robust *z*-score of ≤ -1.5 (159 miRNAs, 9.2% of miRNAs screened) were chosen for further characterization. To narrow down candidate miRNA genes, hits were subjected to several screening passes (**Fig. 1a**, bottom). Briefly, candidates were filtered on the basis of whether they were highly expressed in mouse or human liver (nine miRNAs, 0.52% of miRNAs screened), were active in the liver (eight miRNAs, 0.46% of miRNAs screened) and were previously shown to respond to dietary lipids (five miRNAs, 0.29% of miRNAs screened).

Bioinformatic analysis of miRNA target genes. Target genes for miR-148a were identified and compared using the online target prediction algorithm, miRWalk (http://www.umm.uni-heidelberg.de/apps/zmf/mirwalk/), which provides target interaction information from eight different prediction algorithms. Specifically, the programs miRanda, miRWalk and TargetScan 6.2 were used. Putative targets for miR-148a that were identified by all three of these algorithms (2,217 targets) were uploaded into DAVID v6.7 for functional annotation clustering (http://david.abcc.ncifcrf.gov). 'High' classification stringency settings yielded 398 functional annotation clusters for miR-148a (**Supplementary Table 3**), of which 78 clusters (miR-148a) were highly enriched ($E \geq 1.0$). In another set of analyses, we took the putative targets for miR-148a that were identified above and uploaded them into the gene classification system PANTHER v8.0 (http://www.pantherdb.org) to identify gene targets that mapped to the lipid metabolic process (GO:0006629). The functional interactions of these predicted targets (110 targets for miR-148a) as described in STRING v9.05 (http://string-db.org) were then combined with the functional annotation groups described in DAVID. Matlab and Cytoscape v2.8.3 were used to create the visualization networks, as previously described[41]. STRING interactions with a confidence score of 0.4 or higher were added and are highlighted in gray. Smaller annotation clusters and unconnected genes were left out of the visualization due to space constraints.

siRNA, miRNA mimic and miRNA inhibitor transfections. For siRNA transfections, Huh7 cells were transfected with 20 nM of SMARTpool ON-TARGETplus LDLR siRNA or 20 nM of ON-TARGETplus nontargeting pool for 48 h in LPDS medium or 60 nM of SMARTpool ON-TARGETplus SREBP1 siRNA or 60 nM of ON-TARGETplus nontargeting pool for 60 h as previously described[61]. Verification of *LDLR* and *SREBP1* knockdown was assessed by western blotting and qRT-PCR analysis, as described below. For mimic and inhibitor transfections, Huh7, HepG2 and Hepa cells were transfected with 40 nM miRNA mimic (miR-148a, 5′–UCAGUGCACUACAGAACUUUGU–3′) (Dharmacon #C-300540-05-0005) or with 60 nM miRNA inhibitor (Inh-148a) (Dharmacon #IH-300540-07-0005) using RNAimax (Invitrogen) or Lipofectamine 2000 (Invitrogen) according to previously established protocols[16]. All experimental control samples were treated with an equal concentration of a nontargeting control mimic sequence (CM, 5′–UCACAACCUCCUAGAAAGAGUAGA–3′) (Dharmacon CN-001000-01-20) or inhibitor negative-control sequence (CI, Dharmacon #IN-001005-01-20) for use as controls for non–sequence-specific

doi:10.1038/nm.3949

effects in miRNA mimic or inhibitor experiments. Verification of miR-148a overexpression and inhibition was determined using qRT-PCR, as described below. For dose response experiments, Huh7 cells were transfected with 20 nM of CM or 10, 20, 40 and 60 nM of a miR-148a mimic for 48 h as previously described[16]. In another set of experiments, Huh7 cells were transfected with 40 nM of a miR-148a mimic or 40 nM of a scrambled miR-148a mimic (CM*, 5′–UCUGAGCUCUACAGAACUUUGU–3′). To assess the combined effect of miR-148a overexpression and knockdown of *LDLR*, Huh7 cells were transfected with 60 nM of a nonsilencing siRNA, with 40 nM of a miR-148a mimic or with both for 48 h in LPDS. Cells were transfected with an equal amount of CM to compensate for total DNA content as previously described[23]. For overexpression of nSREBP1c, Huh7 cells were transfected with 1 μg of nSREBP1c (pcDNA3.1-2×FLAG-SREBP1c) or 1 μg of empty vector control (pcDNA3.1) for 24 h using Lipofectamine 2000 (ref. 62). Overexpression was confirmed by qRT-PCR and western blotting.

RNA isolation and quantitative real-time PCR. Total RNA was isolated using TRIzol reagent (Invitrogen) according to the manufacturer's protocol. For mRNA quantification, cDNA was synthesized using iScript RT Supermix (Bio-Rad), following the manufacturer's protocol. Quantitative real-time PCR (qRT-PCR) analysis was performed in triplicate using iQ SYBR green Supermix (Bio-Rad) on an iCycler Real-Time Detection System (Bio-Rad). The mRNA level was normalized to *GAPDH* or 18S rRNA as housekeeping genes. For miRNA quantification, total RNA was reverse-transcribed using the miScript II RT Kit (Qiagen). Primers specific for human and mouse *pre-Mir148a* and *Mir148a* (Qiagen) were used, and values were normalized to *SNORD68* (Qiagen) or 18S rRNA as housekeeping genes. For mouse tissues, total liver RNA from wild-type mice fed a high-fat diet (HFD) was isolated using the Bullet Blender Homogenizer (Next Advance) in TRIzol. One microgram of total RNA was reverse-transcribed and gene or miRNA expression was assessed as above. Primer sequences are available upon request.

Western blot analysis. Cells were lysed in ice-cold buffer containing 50 mM Tris-HCl pH 7.5, 125 mM NaCl, 1% NP-40, 5.3 mM NaF, 1.5 mM NaP, 1 mM orthovanadate, 1 mg/ml of protease inhibitor cocktail (Roche) and 0.25 mg/ml 4-(2-aminoethyl)-benzenesulfonyl fluoride (AEBSF; Roche). Cell lysates were rotated at 4 °C for 1 h before insoluble material was removed by centrifugation at 12,000*g* for 10 min. Nuclear extracts were prepared using the NE-PER Nuclear Protein Extraction Kit (Thermo Scientific) according to the manufacturer's instructions. After normalizing for equal protein concentration, cell lysates were resuspended in SDS sample buffer before separation by SDS-PAGE. After overnight transfer of the proteins onto nitrocellulose membranes, the membranes were blocked with 5% BSA (wt/vol) in wash buffer and probed overnight at 4 °C with antibodies to the following proteins: ABCA1 (1:1,000), LDLR (1:1,000), HSP90 (1:1,000), SREBP1 (1:1,000) and p84 (1:1,000). Blots were then washed and incubated with fluorescently labeled secondary antibodies (Invitrogen). Protein bands were visualized using the Odyssey Infrared Imaging System (LI-COR Biotechnology). Densitometry analysis of the gels was carried out using ImageJ software from the NIH (http://rsbweb.nih.gov/ij/).

For western blot analysis of APOB100 and APOB48 in lipoprotein fractions, an equal volume of three fractions was mixed with reducing SDS sample buffer and separated on a NuPAGE Novex 4–12% Tris-Acetate Mini Gel using 1× NuPAGE Tris-acetate SDS running buffer (Invitrogen). Following overnight transfer of proteins onto nitrocellulose membranes, the membranes were blocked in 5% (wt/vol) nonfat milk dissolved in wash buffer. The membranes were probed with an antibody against APOB (1:2,000) overnight at 4 °C, washed, incubated with fluorescently labeled secondary antibodies and visualized as above. Western blot analysis of APOA1 (1:1,000) in pooled lipoprotein fractions was also carried out in this manner.

Northern blot analysis. miRNA expression was assessed by northern blot analysis as previously described[63]. Briefly, total RNA (5 μg) was separated on a 15% acrylamide Tris-borate-EDTA (TBE) 8 M urea gel and blotted onto a Hybond N+ nylon filter (Amersham Biosciences). DNA oligonucleotides complementary to mature miR-148a-3p (5′-ACAAAGTTCTGTAGTGCACTGA-3′) were end-labeled with [α-^{32}P] ATP and T4 polynucleotide kinase (New England Biolabs) to generate high-specific-activity probes. Hybridization was carried out according to the ExpressHyb (Clontech) protocol. Following overnight membrane hybridization with specific radiolabeled probes, membranes were washed once for 30 min at 42 °C in 4× SSC and 0.5% SDS and subjected to autoradiography. Blots were reprobed for 5S rRNA (5′–CAGGCCCGACCCTGCTTAGCTTCC GAGAGATCAGACGAGAT–3′) to control for equal loading.

Ribonucleoprotein immunoprecipitation (RNP-IP). AGO2 immunoprecipitation (AGO2-IP) experiments after CM or miR-148a transfection were conducted in Huh7 cells as previously described[64]. Briefly, 1×10^7 cells were transfected with 20 nM miR-148a or CM using RNAimax for 24 h. After 24 h, cells were collected and subjected to AGO2-IP using the RNA isolation kit for human AGO2 (Wako Chemicals) according to the manufacturer's instructions. The IP pulldown RNA was used to determine the expression levels of *MIR148A* and *LDLR* by qRT-PCR, as described above.

In another set of experiments, RISC complexes were immunoprecipitated from the livers of mice that were fasted for 24 h or fasted for 24 h and re-fed a high-carbohydrate–low-fat diet for 12 h using 5 μg of either an antibody against mouse Ago2 (2D4, Wako) or an IgG control antibody (Cell Signaling) as previously described[65]. Ago2-bound RNA was used to determine the expression levels of *Mir148a*, *Abca1* and *Ldlr* mRNA as described above. Genes not predicted to be targets of miR-148a (*Rn18S*, *Actb* and *Rplp0*) were used as negative controls.

Chromatin immunoprecipitation (ChIP) assays. Equal portions of frozen liver tissue (~100 mg each) from fasted and re-fed mice were pooled ($n \geq 2$ mice per group) and crushed into powder in liquid nitrogen. Liver powders were transferred into microcentrifuge tubes and homogenized in cold 1× PBS plus protease inhibitors. Following homogenization, samples were filtered, resuspended in 10 ml 1× PBS containing 1% formaldehyde and rotated on a shaker for 10 min at room temperature (RT). To quench formaldehyde, glycine was added to a final concentration of 0.125 M and samples were rotated for an additional 5 min at RT. Cells were then collected by centrifugation, washed twice in cold 1× PBS plus protease inhibitors and incubated in 2 ml cold ChIP lysis buffer 1 (50 mM HEPES pH 7.6, 140 mM NaCl, 1 mM EDTA, 10% glycerol, 0.5% NP-40, 0.25% Triton X-100) for 10 min at 4 °C. The samples were then centrifuged at 3000*g* at 4 °C for 5 min, incubated with 2 ml cold ChIP lysis buffer 2 (10 mM Tris-HCl pH 8, 200 mM NaCl, 1 mM EDTA, 0.5 mM EGTA) for 10 min at 4 °C and centrifuged at 3,000*g* for 5 min at 4 °C. The supernatant was removed and the pellet of nuclei was resuspended in 270 μl ChIP lysis buffer 3 (10 mM Tris-HCl pH 8, 0.5% sarkosyl, 0.5 mM EGTA, 1 mM EDTA, 100 mM NaCl, 0.1% sodium deoxycholate). Nuclear lysates were sonicated 3 × 5 min (30 s on and 30 s off) on high using a Diagenode Biorupter (Diagenode, cat #: UCD-200 TO). After checking chromatin size by agarose gel electrophoresis, extracts were clarified by centrifugation at maximum speed for 10 min at 4 °C, precleared with 60 μl of Protein G beads (Millipore #16-201) for 1 h at 4 °C and then incubated overnight at 4 °C with 4 μg of anti-SREBP1 or control rabbit IgG. Antibody-bound complexes were then captured by incubation with 60 μl of Protein G beads for 1 h at 4 °C. Beads were washed once with low-salt immune complex wash buffer (0.10% SDS, 1% Triton X-100, 2 mM EDTA, 20 mM Tris-HCl pH 8.1, 150 mM NaCl), once with high-salt immune complex wash buffer (0.10% SDS, 1% Triton X-100, 2 mM EDTA, 20 mM Tris-HCl pH 8.1, 500 mM NaCl), twice with LiCl immune complex wash buffer (0.25 M LiCl, 1% NP-40, 1% deoxycholic acid, 1 mM EDTA, 10 mM Tris-HCl) and once with TE (10 mM Tris-HCl pH 8, 1 mM EDTA). Antibody-bound complexes were then eluted by incubation with 200 μl of elution buffer (100 mM $NaHCO_3$, 1% SDS) for 15 min with gentle rotation followed by a second 15-min elution with 200 μl of elution buffer. To reverse crosslinks, the eluates were combined, treated with 5 M NaCl and incubated overnight at 65 °C. Samples were then incubated with 1 μl RNase A, incubated for 30 min at 37 °C and treated with 4 μl 0.5 M EDTA, 8 μl 1 M Tris-HCl and 1 μl proteinase K for 1 h at 45 °C. DNA was purified using the QIAquick PCR Purification Kit (QIAGEN) according to the manufacturer's instructions and eluted in 50 μl of TE buffer. qPCR was run as described above using primer sets for the following promoters: *Fasn* (5′-GCGCAGCCCCGACGCTCATT-3′ and 5′-CGGCGCTATTTAAACC GCGG-3′) and *Srebf1* (5′-GTAGCCAATGGGTGCAAGG-3′ and 5′-CACGTG ACCAAAACCAGAGT-3′). Two primer sets were used for the *Mir148a* promoter,

both of which gave similar results (5′-AATAAGAGCGCAGGTCGTC-3′ and 5′-GCTGAGCTAGGCTTCCAGT-3′; 5′-GGAACCTGCTGACTTGACAC-3′ and 5′-GACGACCTGCGCTCTTATT-3′). A primer set amplifying a region upstream of the predicted SREBP1-binding sites in the *Mir148a* promoter, uNEG (5′-AAACGCATTGCCATTCTC-3′ and 5′-ATTTCAGTAGCTCAAGCACAG-3′), was used as a negative control. Data was normalized using the percentage input method and plotted relative to that of the IgG control.

Low-density lipoprotein receptor activity assays. Human LDL was isolated and labeled with the fluorescent probe DiI as previously reported[66]. Huh7 cells were transfected in 6- or 12-well plates with miRNA mimics and inhibitors in DMEM containing 10% LPDS for 48 h. Cells were then washed once in 1× PBS and incubated in fresh media containing DiI-LDL (30 μg/ml cholesterol). Nonspecific uptake was determined in extra wells containing a 50-fold excess of unlabeled native LDL (nLDL). Cells were incubated for 8 h at 37 °C to allow for DiI-LDL uptake in screening optimization experiments and for 2 h at 37 °C for subsequent validation experiments. In other instances, cells were incubated for 90 min at 4 °C to assess DiI-LDL binding. At the end of the incubation period, cells were washed, resuspended in 1 ml of PBS and analyzed by flow cytometry (FACScalibur, Becton Dickinson), as previously described[67]. The results are expressed in terms of specific median intensity of fluorescence (M.I.F.) after subtracting autofluorescence of cells incubated in the absence of DiI-LDL.

Fluorescence microscopy. For internalization of an antibody specific to LDLR and DiI-LDL uptake assays, Huh7 cells were grown on coverslips and transfected with a MIR148A mimic or negative-control mimic (CM) in DMEM containing 10% LPDS. 48 h post transfection, cells were cooled to 4 °C for 20 min to stop membrane internalization. Cells were then incubated with an LDLR-specific monoclonal antibody (mAb) (clone C7, Santa Cruz) and 30 μg/ml DiI-LDL for 40 min at 4 °C. Following incubation, cells were gently washed twice with cold medium and shifted to 37 °C to allow for internalization of both LDLR-antibody complexes and DiI-LDL for the indicated times and fixed with 4% PFA. After 5 min of permeabilization with 0.2% Triton X-100 0.2% and 15 min of blocking (PBS, 3% BSA), cells were stained with Alexa Fluor 488–conjugated anti–mouse IgG (Molecular Probes) and TO-PRO-3 iodide (Life Technologies) for 1 h at room temperature. After this, cells were washed twice with 1× PBS and mounted on glass slides with Prolong-Gold (Life Technologies). For LDLR-GFP rescue experiments, Huh7 cells were grown on coverslips and cotransfected with 1 μg *LDLR*-GFP and 40 nM of CM or miR-148a mimic. 48 h post transfection, cells were incubated with 30 μg/ml DiI-LDL for 2 h at 37 °C (for uptake) or with 30 μg/ml DiI-LDL for 90 min at 4 °C (for binding). Cells were then washed twice with 1× PBS, fixed with 4% PFA and blocked (3% BSA in 1× PBS) for 15 min. Following this, cells were washed twice and mounted on glass slides with Prolong-Gold (Life Technologies). All images were analyzed using confocal microscopy (Leica SP5 II) equipped with a 63× Plan Apo lens. All acquisition parameters of comparable images were maintained constant. Image analysis was performed using ImageJ (NIH) and Adobe Photoshop CS5.

3′ UTR luciferase reporter assays. cDNA fragments corresponding to the entire 3′ UTR of human *LDLR* and *ABCA1* were amplified by RT-PCR from total RNA extracted from HepG2 cells using XhoI and NotI linkers. The PCR product was directionally cloned downstream of the *Renilla* luciferase open reading frame of the psiCHECK2 vector (Promega). This vector also contains a constitutively expressed firefly luciferase gene, which is used to normalize transfections. Point mutations in the seed region of the predicted miR-148a–binding sites within the 3′ UTR of *LDLR* and *ABCA1* were generated using the Multisite-Quickchange Kit (Stratagene), according to the manufacturer's protocol. All constructs were confirmed by sequencing. COS7 cells were plated into 12-well plates and cotransfected with 1 μg of the indicated 3′ UTR luciferase reporter vectors and miR-148a mimics or control mimics (Life Technologies) using Lipofectamine 2000 (Invitrogen), as previously described[16]. After 24 h of transfection, luciferase activity was measured using the Dual-Glo Luciferase Assay System (Promega). *Renilla* luciferase activity was normalized to the corresponding firefly luciferase activity and plotted as a percentage of the control (cells cotransfected with the corresponding concentration of control mimic). Experiments were performed in triplicate wells of a 12-well plate and repeated at least three times.

***MIR148A* promoter assays.** A 2.3-kb fragment of the human *MIR148A* promoter was amplified by PCR from the BAC clone RP11-184C17 with the following primers: 5′-TGATGGCAGACAATAACTCC-3′ and 5′-AAAGT GCTTTCCCATCTTCC-3′. The PCR product was directionally cloned into a PGL3 promoter vector (Promega) using the KpnI and HindIII linkers. For overexpression assays, HeLa cells were cotransfected with 0.5 μg of the indicated p148a-luc constructs, 0.01 μg of *Renilla* luciferase reporter plasmid and 0.5 μg of nuclear SREBP1c or empty vector control using Lipofectamine 2000. For dose-response experiments, HeLa cells were cotransfected with 0.5 μg of p148a-luc, 0.01 μg of a *Renilla* luciferase reporter plasmid, and 0.5, 1 or 2 μg of nuclear *SREBP1c* or empty vector control using Lipofectamine 2000. After 24 h of transfection, luciferase activity was measured using the Dual-Glo Luciferase Assay System (Promega). *Renilla* luciferase activity was normalized to the corresponding firefly luciferase activity and plotted as a percentage of the control (cells cotransfected with the corresponding concentration of empty vector control) as previously described[68]. Experiments were performed in triplicate wells of a 12-well plate and repeated at least four times. For assays with T090, Huh7 cells were co-transfected with 0.5 μg of p148a-luc and 0.01 μg of *Renilla* luciferase reporter plasmid using Lipofectamine 2000. 24 h after transfection, cells were washed and treated with vehicle or 3 μM T090 for 12 h. Experiments were performed in triplicate wells of a 12-well plate and repeated at least three times. Luciferase activity was measured as described above and plotted as a percentage of the control (cells treated with vehicle). Experiments were performed in triplicate wells of a 12-well plate and repeated at least three times.

Cholesterol efflux assays. Cholesterol efflux assays were performed as previously described[69]. Briefly, Huh7 cells were seeded at a density of 2×10^5 cells per well and transfected with either CM, miR-148a, CI or Inh-148a. After 48 h of transfection, cells were loaded with 0.5 μCi/ml [^{3}H]cholesterol (PerkinElmer) for 24 h. 12 h after loading, cells were incubated with 3 μM T090 to increase the expression of *ABCA1*. Then cells were washed twice with PBS and incubated in DMEM supplemented with 2 mg/ml fatty acid–free BSA (FAFA-media) (Sigma) in the presence of an ACAT inhibitor (2 μmol/liter) (Sandoz 58-035, Sigma-Aldrich) for 4 h before the addition of 50 μg/ml human APOA1 in FAFA-media with or without the indicated treatments. Supernatants were collected after 6 h and the level of [^{3}H]cholesterol was quantified by scintillation counting. Values are expressed as a percentage of total cell [^{3}H]cholesterol content (total effluxed [^{3}H]cholesterol + cell-associated [^{3}H]cholesterol).

Cellular cholesterol measurements. Huh7 cells were seeded at a density of 5×10^5 cells per well and transfected with CM, miR-148a, CI or Inh-148a. 48 h after transfection, cells were incubated with 30 μg/ml nLDL for 2 h. Intracellular cholesterol content was measured using the Amplex Red Cholesterol Assay Kit (Molecular Probes, Invitrogen), according to the manufacturer's instructions.

Mouse studies. Male C57BL/6 mice were purchased from Jackson Laboratories (Bar Harbor, ME) and kept under constant temperature and humidity under controlled dark (12 h) and light (12 h) cycles. For HFD studies, 8-week-old male mice ($n = 6$ per group) were placed on a chow diet or an HFD containing 0.3% cholesterol and 21% (wt/wt) fat (Dyets, Inc.) for 3 weeks. Liver samples were collected as previously described[16] and stored at −80 °C until total RNA was harvested for miRNA expression analysis.

*APOB*Tg;*Ldlr*$^{-/+}$ mice were generated by breeding *APOB*Tg male mice (Taconic) with female *Ldlr*$^{-/-}$ (Jackson) mice. For miR-148a inhibition experiments, 8-week-old male *APOB*Tg;*Ldlr*$^{-/+}$ mice fed a chow diet were randomized into two groups: LNA control ($n = 10$) and LNA anti–miR-148a ($n = 10$). Mice received intraperitoneal (i.p.) injections of 5 mg per kg body weight LNA control (5′–ACGTCTATACGCCCA–3′) or LNA anti–miR-148a (5′–TTCTGTAGTGCACTG–3′) oligonucleotides (Exiqon) every 3 d for a total of 2 weeks. 24 h after the final injection, mice were euthanized and hepatic gene expression was analyzed (see above). In another set of experiments, 8-week-old male *APOB*Tg;*Ldlr*$^{-/+}$ mice ($n = 5$ per group) were treated and fed a chow diet as above for 2 weeks, at which point the mice were switched to a HFD (60% fat, Research Diets D12492) and given weekly i.p. injections of LNA control or LNA anti–miR-148a oligonucleotides for 4 weeks. One week after the last injection, the mice were euthanized and hepatic gene expression was analyzed. All animal

doi:10.1038/nm.3949

experiments were approved by the Institutional Animal Care Use Committee of the Yale University School of Medicine. 8-week-old male obese (C57BL/6-*ob*/*ob*) mice (Jackson) were maintained as previously described[53]. For fasting and re-feeding experiments, 8-week-old male C57BL/6 mice were divided into three treatment groups as previously described: *ad libitum* (n = 4), fasted for 24 h (n = 9) or fasted for 24 h then re-fed a high-carbohydrate, low-fat diet (TD 88122, Harlan Teklad Diets) for 12 h (n = 9) as previously described[55]. After euthanization, hepatic miRNA and gene expression were analyzed as above.

Primary mouse hepatocyte isolation and culture. For analysis of miR-148a expression, nonfasted 8-week-old male C57BL/6 mice were killed and primary hepatocytes were isolated by isopycnic centrifugation as previously described[70]. On day 0, isolated hepatocytes were plated onto 6-well collagen I–coated dishes (400,00 cells per well) in 2 ml Adherence Medium (Williams' Medium E containing 5% FBS (FBS), 2% penicillin-streptomycin, 10 mM HEPES buffer, 8 µg/ml gentamicin, 1 µM dexamethasone and 1 nM insulin). After incubation for 6 h at 37 °C and 5% CO_2, the attached cells were washed once with 1 ml 1× PBS and then incubated for 14–16 h in 2 ml Maintenance Medium (Williams' Medium E containing 5% FBS (FBS), 2% penicillin-streptomycin, 8 µg/ml gentamicin, 1 µM dexamethasone and 1 nM insulin). On day 1, the cells in each well were washed once with 2 ml 1× PBS, after which the cells received 2 ml of fresh Maintenance Medium supplement with 3 µM vehicle or T090. After incubation for 12 h at 37 °C and 5% CO_2, RNA and protein were harvested for qRT-PCR and western blotting analyses as described above.

Nonhuman primate studies. 7–13-year-old male rhesus monkeys (*Macaca mulatta*) were fed a standard (TestDiet #5038; Purina Mills) or high-fat, high-sucrose diet (42% kcal in fat, Custom formula #07802; Harlan, Teklad, Madison, WI) for two years (n = 4 per group) and maintained as previously described[71]. Animal procedures were approved by the Animal Care and Use Committee of the National Institute on Aging (NIA) Intramural Research Program. After euthanization, liver RNA was isolated using the Bullet Blender Homogenizer (Next Advance) in TRIzol. For mRNA quantification, 1 µg of total RNA was reverse-transcribed using iScript RT Supermix (Bio-Rad) and iQ SYBR green Supermix (Bio-Rad). Quantification of miR-148a was assessed as described above.

Plasma lipid analysis and lipoprotein profile measurements. Blood samples for lipid analysis were collected by retro-orbital venous plexus puncture after a 12-h overnight fast at day 1 and day 14 (for chow diet studies) and at day 1, day 14 and day 43 (for HFD studies). Plasma was separated by centrifugation and stored at 4 °C. The lipid distribution in plasma lipoprotein fractions (pooled plasma, n = 5 per group) was assessed by fast-performance liquid chromatography (FPLC) gel filtration with two Superose 6 HR 10/30 columns (Pharmacia) as previously described[23]. Cholesterol in each fraction was enzymatically measured using the Cholesterol Assay Kit (Wako Diagnostics). Total plasma cholesterol, HDL-C, LDL-C and triglycerides were enzymatically measured (Wako Diagnostics) according to the manufacturer's instructions. Additionally, LDL-C levels were confirmed by subtracting HDL-C from total cholesterol levels. Plasma alanine aminotransferase (ALT), aspartate aminotransferase (AST), albumin and total bilirubin were analyzed in LNA control mice and mice treated with LNA anti–miR-148a (n = 5 per group) by the Yale University School of Medicine Mouse Metabolic Phenotyping Center (MMPC).

Liver histology and hepatic lipid analysis. For histological analysis, mouse livers were perfused with PBS and fixed overnight with 4% paraformaldehyde (PFA) at 4 °C. After incubation, livers were washed with 1× PBS, incubated in 30% sucrose for 24 h, embedded in OCT and frozen. Serial sections (8 µm in thickness) were cut using a cryostat. Every third slide from the serial sections was stained with H&E and each consecutive slide was stained with Oil Red O for visualization of neutral lipids as previously described[72]. Lipids were extracted from 1 mg of liver tissue LNA control mice and mice treated with LNA anti–miR-148a (n = 5 per group) as previously described[73]. Triglyceride and cholesterol content were measured using kits from Wako Diagnostics according to the manufacturer's protocols.

Statistics. Animal sample size for each study was chosen on the basis of literature documentation of similar well-characterized experiments[16,53,55,71]. The number of animals used in each study is listed in the figure legends and in the main text. No inclusion or exclusion criteria were used and studies were not blinded to investigators or formally randomized. *In vitro* experiments were routinely repeated at least three times unless otherwise noted. All data are expressed as mean ± s.e.m. Statistical differences were measured using an unpaired two-sided Student's t-test or one-way ANOVA with Bonferroni correction for multiple comparisons or Student-Newman-Keuls analysis when appropriate. Normality was checked using the Kolmogorov-Smirnov test. A nonparametric test (Mann-Whitney) was used when data did not pass the normality test. A value of $P \leq 0.05$ was considered statistically significant. Data analysis was performed using GraphPad Prism Software Version 5.0a (GraphPad, San Diego, CA).

61. Ramírez, C.M. *et al.* MicroRNA 33 regulates glucose metabolism. *Mol. Cell. Biol.* **33**, 2891–2902 (2013).
62. Dávalos, A. *et al.* miR-33a/b contribute to the regulation of fatty acid metabolism and insulin signaling. *Proc. Natl. Acad. Sci. USA* **108**, 9232–9237 (2011).
63. Suárez, Y., Fernandez-Hernando, C., Pober, J.S. & Sessa, W.C. Dicer-dependent microRNAs regulate gene expression and functions in human endothelial cells. *Circ. Res.* **100**, 1164–1173 (2007).
64. Goedeke, L. *et al.* A regulatory role for microRNA 33* in controlling lipid metabolism gene expression. *Mol. Cell. Biol.* **33**, 2339–2352 (2013).
65. Allen, R.M., Marquart, T.J., Jesse, J.J. & Baldan, A. Control of very low–density lipoprotein secretion by *N*-ethylmaleimide–sensitive factor and miR-33. *Circ. Res.* **115**, 10–22 (2014).
66. Calvo, D., Gomez-Coronado, D., Suarez, Y., Lasuncion, M.A. & Vega, M.A. Human CD36 is a high-affinity receptor for the native lipoproteins HDL, LDL and VLDL. *J. Lipid Res.* **39**, 777–788 (1998).
67. Suárez, Y. *et al.* Synergistic upregulation of low-density lipoprotein receptor activity by tamoxifen and lovastatin. *Cardiovasc. Res.* **64**, 346–355 (2004).
68. Chamorro-Jorganes, A., Araldi, E., Rotllan, N., Cirera-Salinas, D. & Suarez, Y. Autoregulation of glypican-1 by intronic microRNA-149 fine tunes the angiogenic response to FGF2 in human endothelial cells. *J. Cell Sci.* **127**, 1169–1178 (2014).
69. Ramirez, C.M. *et al.* MicroRNA-758 regulates cholesterol efflux through post-transcriptional repression of ATP-binding cassette transporter A1. *Arterioscler. Thromb. Vasc. Biol.* **31**, 2707–2714 (2011).
70. Wang, W. *et al.* Radixin is required to maintain apical canalicular membrane structure and function in rat hepatocytes. *Gastroenterology* **131**, 878–884 (2006).
71. Mattison, J.A. *et al.* Resveratrol prevents high fat/sucrose diet-induced central arterial wall inflammation and stiffening in nonhuman primates. *Cell Metab.* **20**, 183–190 (2014).
72. Goedeke, L. *et al.* Long-term therapeutic silencing of miR-33 increases circulating triglyceride levels and hepatic lipid accumulation in mice. *EMBO Mol. Med.* **6**, 1133–1141 (2014).
73. Miller, A.M. *et al.* MiR-155 has a protective role in the development of non-alcoholic hepatosteatosis in mice. *PLoS ONE* **8**, e72324 (2013).